Immune cell profiling in COVID-19 recovered patients using mass cytometry

Master thesis in Pharmacy

Manpreet Kour Hans

Centre for Pharmacy and

Department of Clinical Science

University of Bergen

May 2020

Acknowledgment

Firstly, I would like to express my very great appreciation and gratitude to my main supervisor Jørn Skavland for his valuable and patient guidance throughout the learning process, in technical training, enthusiastic encouragement, and critical input. The support and everlasting motivation you have given are inestimable and will always be remembered.

Secondly, I want to thank my co-supervisor Silke Appel who recruited me for this project and has guided me throughout the year. Your outstanding suggestions have really motivated and guided me during this hectic period.

I would like to thank all the members at Broegelmanns research group for answering all my questions and everyone teaching in the HUIMM320 course. Especially, thanks to Kjerstin and Marianne for valuable technical assistance during lab experiments. I also want to thank Brith Bergum for your positive energy and for always telling me where Jørn is.

Thank you to my fellow pharmacy students for 5 amazing and memorable years. Victoria and Ingvild your support in the lab and candid conversations have been highly appreciated.

Finally, I want to send a huge thanks to my family for always encouraging, loving, and supporting me during these 5 years. Thank you for making me believe in myself and always fulfilling my wishes.

Thank you!

I hope you have a good time reading through my thesis.

Manpreet Kour Hans

Bergen, May 2020

Abstract

Coronavirus disease 2019 (COVID-19), caused by the zoologic virus severe acute respiratory syndrome coronavirus 2 (SARS-CoV-2), is among the most impactful pandemics in modern history. Infection impact has variating tendency within patients that experience mild disease compared to severely affected patients, such as respiratory failure and death. Currently, treatment strategies aim to alleviating the symptoms, but a healing cure except vaccination is not resolved yet, due to lack of knowledge about the virus and how it affects the immune system. Duration of immunological memory after experiencing COVID-19 is unclear and unknown, along with limited knowledge about the disease grade influence on the immune system recovery.

Firstly, this thesis aimed to study the peripheral blood immune system in SARS-Cov-2 infected patients 6 months post-infection. Using a mass cytometric approach, fixed whole blood in SARS-Cov-2 infected patients and healthy controls were analyzed. We compared immune cell frequencies among moderate and severe disease patients compared to healthy controls. A SARS-CoV-2 specific heterogeneity was observed which indicated recovery based on other factors, such as genetics and medical history.

Secondly, we aimed to identify cell-affecting concentrations of randomly selected phytochemicals (Ellagic acid, rumic acid, Dinatin 7-glucuoronide, and plantainoside D) that can potentially be used in COVID-19 treatment. MTT (3-(4, 5-dimethylthiazolyl-2)-2, 5-diphenyltetrazolium bromide) assay was exploited to find concentrations that affected the cell proliferation on human embryonic kidney cells (HEK293), human embryonic kidney cells variant that express a temperature- sensitive allele of SV40 T antigen (HEK-293t) and colorectal adenocarcinoma cells 2 (CACO-2).

Abbreviations

ACE2	Angiotensin-converting enzyme II
APC	Antigen presenting cell
BCR	B cell receptor
CACO-2	Colorectal adenocarcinoma cells 2
CatB	Cathepsin B
CoV	Coronavirus
COVID-19	Coronavirus disease 2019
D7G	Dinatin 7-glucuoride
DAMP	Damage associated molecular patterns
DC	Dendritic cells
DMEM	Dulbecco's Modified eagle medium
dsRNA	Double stranded RNA
EA	Ellagic acid
FDR	False discovery rate
FBS	Fetal bovine serum
FCS	Furin cleavage cite
HC	Healthy control
HEK	Human embryonic kidney
ICP	Inductively coupled plasma
IFN	Interferon
Ig	Immunoglobulins
IL	Interleukin
MERS-CoV	Middle east respiratory syndrome
MHC	Major histocompatibility complex
MTT	(3-(4, 5-dimethylthiazolyl-2)-2, 5-diphenyltetrazolium bromide)
NET	Neutrophil extracellular traps
NK	Natural Killer cell
PAMP	Pathogen associated molecular patterns
PBMC	Peripheral blood mononuclear cells
PD	Plantainoside D
PFA	Paraformaldehyde
PICS	Post-intensive care syndrome

PPR	Pathogen pattern receptor
RA	Rumic Acid
RBD	Receptor binding domain
RIG-I	Retinoic acid inducible gene I
RLR	RIG-1 like receptors
RTC	Replicase transcriptase complex
RT-PCR	Real time polymerase chain reaction
SARS-CoV	Severe acute respiratory syndrome
ssRNA	Single stranded RNA
TCR	T cell receptor
Tfh	T follicular helper cell
Th1	T helper cell 1
Th17	T helper cell 17
Th2	T helper cell 2
TLR	Toll like receptor
TMPRSS2	Transmembrane protease serine 2
TNF	Tumor necrosis factor
T_{regs}	T regulatory cells

Content

List over figures

1. Introduction

1.1. The immune system

The immune system has advanced mechanisms and many different important components that together protect an individual against harmful pathogens, such as viruses, bacteria, fungi, and parasites. The immune system is divided into two interconnecting branches, the innate immune system and the adaptive system. Both systems work cooperatively together. The innate immune system is congenital and is developed before birth and is the first line of defense (1).

Since the innate immune system is the first line of defense it is dominating in the first hours/days of fighting an antigen. In contrast, the adaptive system must be slowly developed and is not inherited (figure 1). This system has a great capacity to develop an immunological memory. Generally, the innate immune system is non-specific, while the adaptive immune system is more advanced and specific (1).

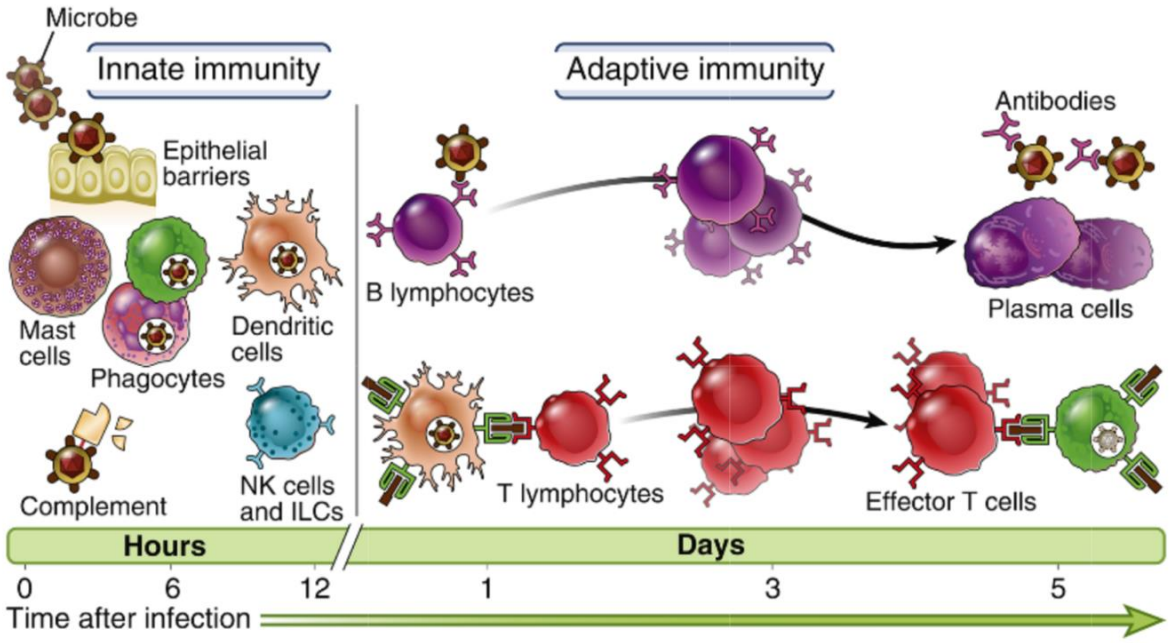

Figure 1 Innate and adaptive immunity. *The innate immune response occurs within hours after infection, while the adaptive immune responses appear later. Figure adapted from (1) and reprinted with permission from Elsevier.*

Innate and adaptive immunity activates different immune cells that can result in cytokine production. Cytokines are messenger molecules that regulate the immune system by suppressing or inducing the immune responses, and it has a major role in orchestrating the

balance between innate and adaptive immunity. These molecules bind to cell receptors and induce complex signalling cascade (1).

Cytokines can have autocrine (effect on the secreting cell), paracrine (effect on other cells), juxtracrine (on adjacent cells, needs membrane anchored proteins), or endocrine (distanced target cells) effects (1). These pleiotropic proteins are divided into proinflammatory (e.g., type 1 interferons/INF-1, tumor necrosis factor/TNF, interleukin/IL-1, IL-12) and anti-inflammatory cytokines (e.g., IL-4, IL-10, transforming growth factor β/TGFβ). However, a cytokine can have both activities dependent on the local microenvironment (1, 2).

1.1.1 Innate immune system

The innate immune system is congenital and has briefly three important functions: inflammation, antiviral response, and stimulation of the adaptive immune system. The innate immune response does not develop immunological memory in the same manner as the adaptive immune system. Responses provided by the innate immune system are essentially similar in every microbe encounter (1).

As shown in figure 1 the main components of the innate immune system are epithelial barriers, monocytes, dendritic cells (DCs), neutrophils, macrophages, natural killer (NK) cells, and the complement system. Innate immune cells recognize the pathogen-associated molecular patterns (PAMPSs) that have been evolutionarily conserved in microorganisms infecting humans. There are five main pattern recognition receptors (PRR) in the innate immune cells that recognize PAMPS: (Toll-like receptors (TLRs), nucleotide-binding oligomerization domains (NOD-)-like receptor, retinoic acid-inducible gene (RIG-I), DNA sensors, and C-type lectin (1).

One way of activation of the innate immune system is through PAMPs are lipopolysaccharides binding to TLR on antigen presenting cells (APC) and other cells, like endothelial cells. This will lead to proinflammatory cytokines. PAMPs can also be digested and processed in the APCs and then bounded to major histocompatibility complex (MHC) and translocated on the surface of the APC (1). Dying or damaged cells can release endogenous molecules, called damage-associated molecular patterns (DAMPs) that can also bind to PRR (1).

A collection of cell membrane proteins, surface and intracellular, constitutes the complement system, which plays an important role in defeating inflammations and harmful microbes.

Activated complement proteins can affect microbes through opsonization, cell lysis, or with triggering immune cells to produce molecules that result in an inflammation (1).

1.1.2 Adaptive immune system

In contrast to the innate immune system, the adaptive immune system needs to be gained and built up through exposure to different kinds of infections and antigens. When activated the adaptive system provides a specific response against specific pathogens/antibodies based on immunological memory. B lymphocytes and T lymphocytes are the important components in the adaptive immune system. B and T cells have specialized antigen-specific receptors. Adaptive immune system is divided into two response types, humoral immunity (mediated of B lymphocyte produce antibodies) and cell-mediated immunity (T lymphocytes) (1).

Upon recognition of a microbial antigen, naive lymphocytes proliferate and differentiate into effector or memory cells. Naive T lymphocytes have a unique receptor not responding to self-antigen and have not been presented to its specific antigen by an APC. When a naive T-cell, $CD4^+$ or $CD8^+$ is presented to its antigen by an APC, activation of the T-cell will occur and start an immune response. Of the T-cell clonal expansion, some cells are programmed to be memory cells. Effector $CD4^+$ T cells activate B cells, macrophages, and other cell types through the production of cytokines. Effector $CD8^+$ T cells have the ability to kill infected host cells. B effector lymphocytes are antibody-secreting plasma cells located in the peripheral lymphoid organs, plasmablasts located in the blood, or long-lived plasma cells in the bone marrow (1).

In contrast to effector cells, memory cells remain alive without the presence of antigen, resulting in a higher frequency of memory cells dependent on age. The peripheral blood of adults can contain 50% or more memory cells (figure 2) (1).

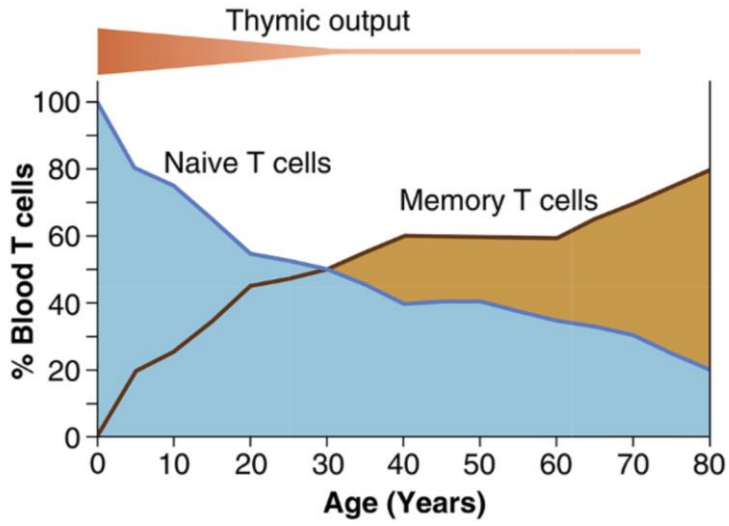

Figure 2 Age-dependent alteration of naive and memory cells. *Figure adapted from (1) and reprinted with permission from Elsevier.*

$CD4^+$ T helper cells are divided into subtypes based on their cytokine production. These subsets have distinct functions and defend against different types of microbial infections (1). Subtypes of T helper (Th) cells are Th1, Th2, Th9, Th17, and T_{FH}. Th1 is essential in IL-2 and IFN-γ mediated activation of macrophage, effector cytotoxic cells, and NK cells. Th2 cells are essential for humoral response, and IL-4 and IL-6 mediate activation of eosinophils, basophils, and mast cells (3).

B lymphocytes mediated the humoral immunity and produce antibodies. Antibodies, also known as immunoglobulins (Ig), can be membrane-bounded on B cells or secreted proteins. Different Ig isotypes (IgD, IgM, IgE, IgG, and IgA) have specific effector, physical, and biologic characteristics. Engagement of membrane-bounded antibodies starts B cell activation and triggers antibody secretion. Stimulation of antibodies triggers a range of effector mechanisms that eliminate the antigen/microbe (1).

Although the immune system is broadly divided into two arms, the systems work together to provide an effective host response. APCs have major histocompatibility complex (MHC) presented on their surface that shows antigen fragments to cells in the adaptive immune system. MHC can be divided into two subclasses, MHC class I and MHC class II. MHC class I is present on every nucleated cell in our body, and MHC class II is only expressed on the DC, macrophages, and B lymphocytes (1).

Even though the lymphocytes are mainly a part of the adaptive immunity, they have has some features that function in the innate immunity. These cells have the same morphological and functional characteristics similar to T cells, but the receptor diversity is limited. γδ T cells and NK-T cells are examples of lymphocytes with limited diversity. NK-T cells express T cell receptors with limited diversity along with NK-cell-specific surface molecules (1).

1.2. CORONAVIRUS

1.2.1 A brief historical perspective of human coronaviruses

The first coronavirus (CoV) was discovered in mid 1960s and has in the past years caused viral outbreaks all over the world. The name is adapted from their characteristic surface crown-like spikes. Normally CoVs circulate in animals, such as camels, cats, pangolin, snakes, and bats, and have the ability to be transmitted between animals and humans (4).

In modern medical history, three types of CoVs have caused viral outbreaks. In 2002 the first CoV, severe acute respiratory syndrome CoV (SARS-CoV) discovered in Guangdong, in southern China caused a pandemic. During this SARS pandemic, 26 countries were affected in different continents. Overall, 8098 infected individuals were reported. In 2012 and 2015 Middle East Respiratory Syndrome CoV (MERS-Cov), which has until today caused 858 deaths since September 2012. Altogether 27 countries were affected. Lately, the SARS-Cov-2 in 2020 (late 2019) and by 15th May 2021 SARS-CoV-2 had caused 3 352 109 deaths worldwide (5-7).

For SARS-CoV-2 it is believed that the disease has transferred from a seafood market that sold live animals in Wuhan, China. Infection with SARS-CoV-2 gives the disease COVID-19 and is developed through transmission through the respiratory tract (8).

1.2.2 SARS-CoV-2

Several different zoonotic viruses cause acute respiratory tract infections in western and developing countries. Annually, there are an estimated one billion zoonotic positive cases every year, and up to millions of deaths yearly (9).

Coronaviruses are identified as a zoonotic virus-containing single stranded RNA, that transmit infection between people and vertebrate animals and is found throughout this world. The three big coronaviruses that have caused fatal consequences have started twice in China and once in middle east (6, 7). SARS-CoV-2 in human and betacoronaviruses in bats are proven until date to be the most closely related, but the intermediate host leading to transmission in humans is still unknown (10, 11).

To survive the mammal immune system, SARS viruses develops virulence factors that manipulate and suppress the immune system. SARS-CoV-2 has developed postponement and hindrance of IFN mediated production of neutralizing antibodies (12). In comparison to SARS-CoV-1, SARS-CoV-2 has an evolutionary gain of FURIN cleavage site (FCS) on the S protein.

As for December 2020, it is believed that FCS is responsible for the tremendous infectivity and transmissibility. For influenza viruses, the FCS has been a significant part of developing high virulence. To what extent it does the same for SARS-CoV-2 is not known yet (13).

SARS-CoV-2 has four characteristic proteins, spike (S), membrane (M), nucleocapsid (N), and envelope (E) proteins as shown in figure 3. S protein binds to the angiotensin-converting enzyme II (ACE2) on epithelial cells located in the lungs (14).

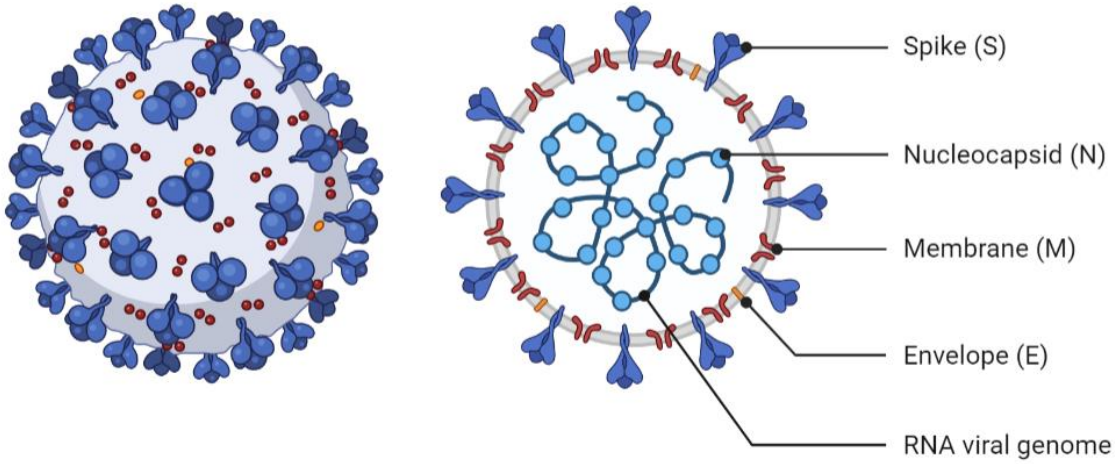

Figure 3 Overview of the SARS-CoV-2 structure. *The figure shows the SARS-CoV-2 structure and the significant proteins that it contains. Figure adapted from BioRender.*

Infection caused by this virus can be spread with contact/droplet, airborne, and fomite transmission, along with other methods of transmission. Contact and droplet transmission is spread with respiratory droplets through coughs, sneezes, and talks with infected people. Touching contaminated surfaces and then eyes, nose or mouth, can lead to fomite transmission. Fomite of liable SARS-CoV-2 virus or RNA analyzed with RT-PCR has shown that SARS-CoV-2 can be found on these surfaces for hours to days, depending on the environment (humidity and temperature) (15).

Airborne and other modes of transmission are under scientific research. The definition of airborne transmission is spread of an infection through exposure of droplets containing virus that can remain in the air for a period and over long distances. For SARS-CoV-2 the possibility for a susceptible person to be infected based on inhaled aerosols is not fully known (11, 16, 17). Other modes of transmission can possibly include urine and feces transmission. SARS-CoV-2

has been detected in biological samples of both urine and feces, but to date, it has not been confirmed if transmission can occur with these pathways (11, 18, 19).

Some individuals have higher risk of getting severe case history, depending on health factors, such as diabetes, high blood pressure, asthma, immune deficiency, age, obesity, dementia, stroke, chronic liver diseases, and stroke (20). Comorbidities have an impact on the disease course and on which scale the disease can be harmful.

Mild to moderate infections leads to fever, dry cough, and tiredness. Aches, pain, sore throat, diarrhea, conjunctivitis, headache, loss of taste or smell, rashes on the skin, and discoloration of fingers or toes are more infrequent symptoms. In severe cases, loss of speech or movement, acute respiratory distress syndrome, multi-organ failure, difficulty breathing, or shortness of breath, and chest pain can occur. In critical severe cases, the disease can lead to respiratory failure and death (5).

New studies suggest that almost one in five infected people are asymptomatic for SARS-CoV-2. Reliable figures are difficult to develop since a clear difference between the asymptomatic patients and pre-symptomatic patients is not fully determined and a standardized definition is not made (21).

One out of five patients with COVID-19 develops long-term effects that last more than 12 weeks, called long COVID (22). Patients who experience a severe disease progression and require intensive care have a higher risk to develop long COVID. However, it is still unclear whether symptoms are caused by COVID-19 or intensive care consequences. Patients who have been undergoing intensive care have normally post-intensive care syndrome (PICS), which has similarities with COVID-19 symptoms. Older age, female sex, and disease severity is a typical risk factor for PICS. Long COVID studies focus on the symptom prevalence, but to what extent these remaining symptoms effect life quality is unknown (23).

1.3.3 SARS-CoV-2 lifecycle

Coronaviruses have a proofreading mechanism that prevents the virus to be weakened. Compared to influenza viruses, coronaviruses swap RNA chunks with other coronaviruses, which gives the coronavirus new unknown sequences for the human immunity.

The S1 protein on SARS-CoV-2 surface binds to angiotensin-converting enzyme II (ACE2) on epithelial cells located in the lungs. S2 mediates then the spike cleaving by transmembrane

protease serine 2 (TMPRSS2) and fusion of the virus into the host cell occurs. Newly discovered is the FURIN proteases helping/priming activity ensuring that the virus enters the host cell (24). Endosomal cysteine proteases cathepsin B (CatB) and CatL assists in the fusion process in a minor order (24).

Immediately after entry into the host cell, the virus releases RNA. The two large genomes ORF1a and ORF1b undergo translation and results in the production of two large polyproteins, pp1a and pp1ab. Papin-like protease (PLpro) and chymotrypsine protease (a serine type Mpro), 3CLpro, supplement the polyproteins. Non-structural proteins (nsp) with different functions are released by the pp1a and pp1ab (figure 4) (20, 25-27).

Nsps are important for intracellular replication and can assemble into replicase-transcriptase complex (RTC). RTC is a key factor for viral RNA transcriptase, leading to S, E, M production in endoplasmic reticulum. Viral components get maturated in Golgi vesicle resulting in mature lipid enveloped virion. By exocytosis, the new virion leaves the cells and will bind to other host cells (28).

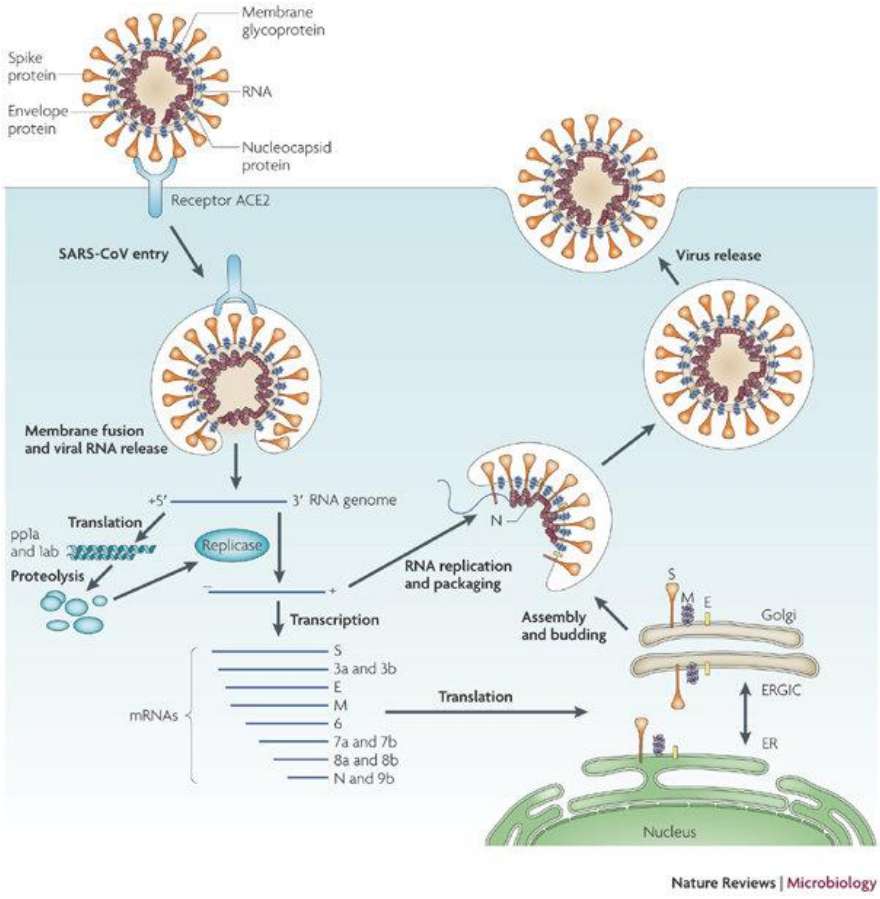

Figure 4 SARS-CoV-2 life cycle phases. *SARS-CoV-2 binds to ACE-2 receptors located on the epithelial cells in the lungs. Conformational changes happen in the S protein, which leads to fusion between the virus and the host cell. Upon entry into the cell, RNA gets released which is translated into essential proteins and viral replicase polyproteins. New virions get produced in the endoplasmic reticulum Golgi intermediate compartment (ERGIC) and then by exocytosis released. Figure adapted from (29) and reprinted with permissions from RightsLink/Springer Nature.*

1.3.4 Diagnosis

Diagnosis and detection of SARS-CoV-2 in patients are done by nasopharyngeal and oropharyngeal swabs. Samples are then carried in a transport media and sent to laboratories to detect the virus in the samples. In most countries, and especially in Norway, the recommendation of diagnosis in people has changed multiple times. Depending on the capacity of the testing that could be conducted. However, it is recommended that everyone experiencing acute respiratory infection symptoms and other symptoms for more than two days should be tested (30).

The diagnostic procedures are done in two ways. Firstly, direct detection of virus in patient samples with for example detection of proteins from the virus by culturing it, with using nucleic acid amplification tests, such as RT-PCR, transcription-mediated amplification), or Loop mediated isothermal amplification (LAMP). Secondly, immunological diagnostics used for identifying the virus-specific antibodies after having the viral infection. (31)

Global standards of detecting SARS-CoV-2 in patient samples are done using real-time polymerase chain reactions (RT-PCR) assays that have high specificity and sensitivity. The specificity is estimated around 99% and sensitivity around 80%. Sensitivity is slightly lower than the specificity because that parameter is dependent on the stage of the disease. The sensitivity of RT-PCR increases if the test is conducted within the onset of symptoms. (30)

However, alternatively, SARS-CoV-2 infections can be detected with antigen rapid-tests. Most of the rapid-tests are mainly based on detecting specific viral antigens depending on the particular test kit. Antigen tests has lower sensitivity hence low antibody count in early phase detection of COVID-19 (32).

1.3.5 Treatment of COVID-19

Treatment of SARS-CoV-2 is not fully specific; however, guidelines are developed that are updated regularly. In the first few first months of 2021, vaccines have been developed and rapid vaccination is happening, although limitations of doses slowdowns the process of developing herd immunity. However, patients who need acute treatments in Norway, get immunosuppressives, such as dexamethasone, prednisolone, or other types of glucocorticoids. If the course of the disease is severe, treatment with antiviral remdesivir can be given. (33)

1.3.6 Immunity against SARS-CoV-2

Understanding of the SARS-CoV-2 immune response is limited and updating rapidly. Along with lack of information about alterations occurring in convalescent patients' immune system. However, the antiviral response against SARS-CoV-2 is believed to be like other CoVs since the homology is similar. (34)

ssRNA and dsRNA from the virus engage the PRR receptors, such as RIG-I like receptors (RLRs) and TLRs, and initiates downstream signalling cascades resulting in cytokine production. In antiviral responses cytokines as INF type I/III, TNF-α, IL-1, IL-6, and IL-18 get released. IFN-1 is believed to limit the CoV infection. (34) However, studies have shown that SARS-CoV-2 has a mutated difference compared to other CoVs, resulting in the ability to block the IFN type I/III production. (34)

IFN levels are delayed in SARS-CoV-2 infected patients. IFN levels correspond to the severity of COVID-19. Due to poor initial IFN response, the recruitment of neutrophils can be postponed. Late recruitment of neutrophils can result in increased viral load (35). In severe COVID-19 patients increased neutrophils was reported by Schulte-Schrepping et.al, 2020 (36).

In severe COVID-19 patients elevated inflammatory cytokines such as IL-6, IFN-γ, TNF-α, IL-8, MCP-1 (CCL2 chemokine ligand 2), and IL-10 have been detected and show resemblance to an inflammatory phenomenon called cytokine storm. Reasons for the cytokine storm occurring are yet to be established. One theory is the viral PAMPs and host danger signals trigger the phenomenon (37).

The knowledge about T cells against SARS-CoV-2 is limited. In peripheral blood, the total number of $CD4^+$ and $CD8^+$ T cells, B cells, and NK cells has been low (3). COVID19 disease outcome is associated with the Th1/Th2 balance. Th1 can discreetly clear the viral infection and lack of its function can lead to exacerbated reaction leads to the cytokine storm. Th2 cells are associated with poor prognosis for the disease. (3)

Acute phases of SARS-CoV-2 infections are associated with significantly marked lymphopenia with low numbers of circulating $CD4^+$ T cells and $CD8^+$ T cells (38). Lymphopenia can be caused by reduction in APCs functions and impaired migration of DCs that lead to limited T cell proliferation (38), this includes decreasing numbers of γδ T cells (39). In SARS-CoV-2 infections γδ T cells act as a bridge between the adaptive and innate immune system since it has an antigen presenting role. Furthermore, these cells have antiviral effects by secreting IFN-γ (40).

$CD4^+$ T cells and $CD8^+$ T cells are associated with viral clearance in primary infections (38). In a previous study, it has been shown that S-reactive $CD4^+$ T cells are present in patients and healthy donors, suggesting that these T cells are already present in our human body. A possible explanation for this is the previously CoV epidemics (41). The S reactive $CD4^+$ T cells in COVID-19 patients co-expresses CD38 and HLA-DR (38). Some studies have shown that GM-CSF and IL-6 expressing $CD4^+$ T cells are more abundant in severe COVID-19 patients that do not need intensive care. (37)

T cells memory has been shown that it can last up to 17 years after SARS-CoV infection, resulting in protection in long-term cross-immunity (38). However, if this is reliable for SARS-CoV-2 is still unknown.

Follicular helper T cells (T_{FH}) play an important role in antibody mediated humoral immunity. In viral infections, T_{FH} aids long-lived memory B cells and plasma cells, which is important for virus-specific neutralizing antibodies (38). In a case study it has been seen that T_{FH}, APCs, activated $CD4^+$ and $CD8^+$ T cells, IgG and IgM had an increasing tendency post symptoms. (38) To understand if SARS-CoV-2 has an impact on T_{FH} must be investigated by analyzing the immune response in peripheral blood.

IgM and IgA have been detected in blood samples from patients as early as 5 days after infection, while IgG has been measured within 14 days in most patients. Seroconversion starts on day 6 after symptom onset (38). SARS-CoV-2 neutralizing antibodies are directed mainly to the viral surface S-protein and the N-protein. These antibodies neutralize viral infections of ACE-2 expressing human cells and tissues (42). In recovered COVID-19 patients considerable amounts of IgG antibody against SARS-CoV-2 have been detected.

1.3 Aims of the study

Specific aim 1: Identifying and evaluating specific immunological responses and correlate the disease course 6 months post-infection and how SARS-CoV-2 patients differ from healthy controls. Understanding how SARS-CoV-2 patient immune cell composition recovers 6 months post-infection. Subgroup patients and compare to healthy controls differ from the healthy controls and from each other.

Specific aim 2: Use MTT assay to determine toxic concentration of 4 different chemical extracted substances that can be used in the treatment against COVID-19.

2. Materials and Methods

2.1 Specific aim 1

2.1.1 Materials

Written informed consent was obtained from all the participants. The protocol for the collection and storing of blood for research purposes was approved by the regional ethical committee (REK number 118664). The study was conducted in accordance with the Declaration of Helsinki Ethical Principles and Good Clinical practices.

2.1.1.1 Recruitment of SARS-CoV-2 infected individuals

Individuals (table 1) who had SARS-CoV-2 in March 2020 were contacted by the Influenza Centre at University of Bergen and asked to take a part in the project "COVID-19 infeksjon: klinisk og immunologisk respons" at UiB. Blood samples will be taken at onset of disease at 6, 12, and 18 months. For this study blood was analyzed from timepoint 6 months post-infection.

2.1.1.2 Recruitment of healthy controls

Ten randomized healthcare workers were recruited for healthy controls (table 1). Blood samples obtained from the healthy controls were part of a research project evaluating vaccination against COVID-19. All samples were taken pre-vaccination against COVID-19.

Table 1 Characteristics of the participants

			COVID-19	
		Control	Moderate	Severe
Groups	n	10	35	14
Sex	M	3	19	7
	F	7	16	7
Age	< 40	5	9	1
	40 – 65	5	18	6
	>65	0	8	7
Comorbidity + BMI	Y	0	13	10
	N	10	22	4

2.1.1.3 Harvesting and stabilizing samples

Full blood samples, including healthy control samples, were stabilized with proteomic stabilizer (Smart Tubes Inc., San Carlos, California, US). Proteomic stabilizer is used for preserving whole blood within short time. When these whole blood samples were taken, around 100 samples were collected. To minimize the sample variation when preserving the cells proteomic stabilizer was chosen.

Blood from patients and controls were collected in BD Vacutainer® EDTA (Becton, Dickinson and Company, Franklin Lakes, New Jersey, US. Within 2 hours, 400 µl was mixed with 1.4x proteomic stabilizer and incubated for 10 minutes and then stored at -80^{o}C in Micronics tubes. Within 2 days samples were transferred to -150^{o}C.

2.1.2 Methods

2.1.2.1 Mass cytometry

The relatively novel analytical technology mass cytometry is the central method used in this study. Mass cytometry or cytometry by Time-of-Flight (CyTOF) is an analysis that quantifies cellular features at single-cell resolutions (43). This relatively new analyzing method was developed in 2009 and is a fusion between flow cytometry and mass spectrometry (43). Flow cytometry has been dominating in single-cell analysis since the 1960s but until recently the methodology has been limited of analyzing more than 15 analytes simultaneously. The limitation for making large panels is the fluorescent spectral signal (44).

In flow cytometry antibodies are conjugated with fluorophores for detection. Spread of light from several probes in the sample will cause issue in detecting and quantifying each probe. The CyTOF technology have overcome the problem with overlapping detection using one detector and dividing them by mass. Little or no issues with channel overlapping gives the technology the ability to set up and analyze panels with more than 40 antibodies (45). In mass cytometry probes are conjugated with heavy-metal isotopes (44). One has chosen metals from rear-earth metals. These metals are never found in biological materials, therefore background “noise” is neglectable. (46)

Prepared, fixed, and stained single cells in suspension are applied to the nebulizer by constant pressure and flow. The nebulizer is pressurized with argon it will transform the cell suspension into a fine mist of tiny droplets, ideally no more than one cell (particle) droplet. The mist is generated inside a heating chamber holding 200^{o}C. In this chamber, all liquid, also water in the cells, is evaporated leaving only dried cells to enter the mass spectrometry (46).

The second part of the CyTOF is inductively coupled plasma spectrometry (IPC-MS). The argon plasma generated holds a temperature around 5000K. This high temperature fully atomizes and ionizes all molecules in the sample, ending up with a cloud of charged ions. The ion cloud holds all components built of a cell and the metal-conjugated antibodies and probes that were used for barcoding and staining. The quadrupole unit removes all organic ions, leaving only a cloud of heavy metal reporter ions used for identifying cells and quantifying the given molecules. (43, 44, 46, 47).

The Time-of-flight (TOF) contains absolutely vacuum (10^{-8}Torr). When ions from the cloud are pushed into the TOF, the vacuum will separate the ions according to mass. Lighter ions reach the detector first. From the push is initiated, one can calculate the given time for each ion to reach the detector by mass. Each time frame/window corresponds to one given isotope by mass, equivalent with a channel in mass cytometry. The high sensitivity for the detector, a discrete-dynode electron multiplier, can identify one single ion. Signal intensity detected for each channel determines the abundance of the isotopes in the cloud. Mass abundance values from each cloud generated are saved as a text file and further converted into a Flow Cytometry Standard (FCS) file. (43, 44, 46, 48, 49)

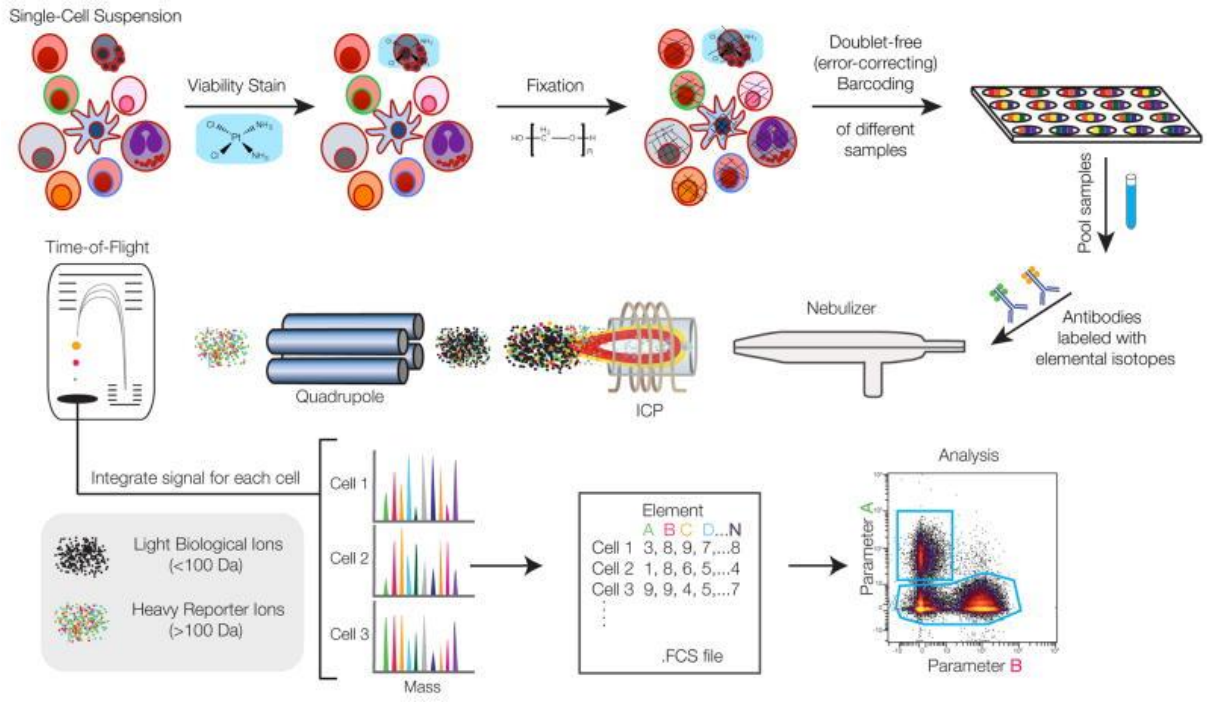

Figure 5 Systemic overview of the mass cytometry process. *Heavy metal labeled antibodies are stained to cells in suspension. These are applied into a capillary system in the mass cytometer.*

The suspension is then taken through the nebulizer, which carries out the single cells. ICP makes ion clouds out of the single cells and the quadrupole removed biological ions. TOF analyzes the remaining ionized ion clouds. Figure adapted from (47) and reprinted with permissions from RightsLink/Springer Nature.

2.1.2.2 Barcoding

Barcoding technique (figure 6) is used for staining all samples with a unique code before combining all of them in one multiplexed sample. There are three main reasons for using this technique; preventing technical variability, reducing volume and antibody consumption, and removing doublets in the analysis. Technical variabilities include washing, volume staining, antibody concentration, temperature variability, and CyTOF acquiring. The individual samples were tagged with heavy metal isotopes combinations, that were unique for the different samples. (50)

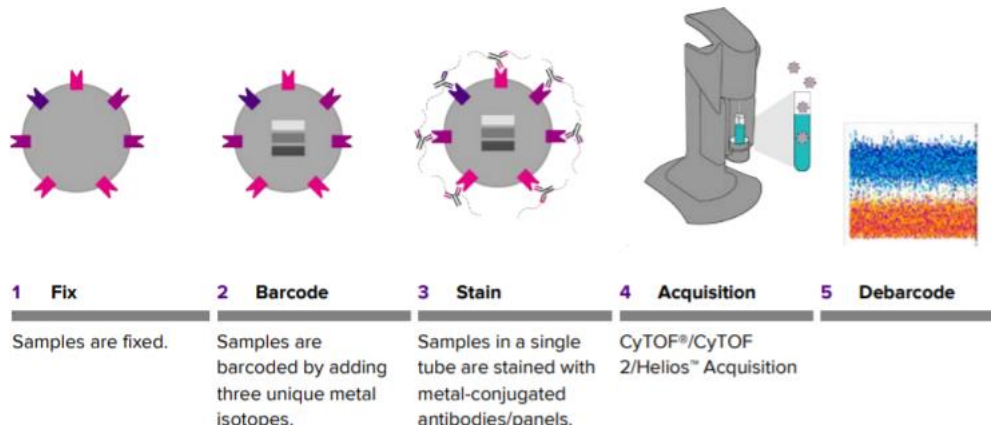

Figure 6 Barcoding workflow**.** *Thawed fixed cells are barcoded with metal isotopes and converted to one multiplex sample. The multiplex sample is stained with metal-conjugated antibodies. Samples will then be acquired by CyTOF® and then debarcoded to single data samples. Figure adapted from (51).*

Palladium (Pd) the most common tags used for barcoding. It is in the lower mass detection range where sensitivity is the lowest. Palladium isotopes are not commercially used as antibody tags, because of its antibody instability (52).

In this project, a 20-plex barcode, set based on Zunder *et.al.* 2015 (49), was made in-house. Six stable palladium isotopes, 102, 104, 105, 106, 108, 110, were used. All samples get a unique combination of 3 palladium isotopes out of 6. In this project four additional isotopes, cisplatin (Pt) 194, 195, 196, and 198 were used 2 out of 4 for combining the three 20-plex barcodes. The schematic setup and all barcode combinations are shown in figure 7.

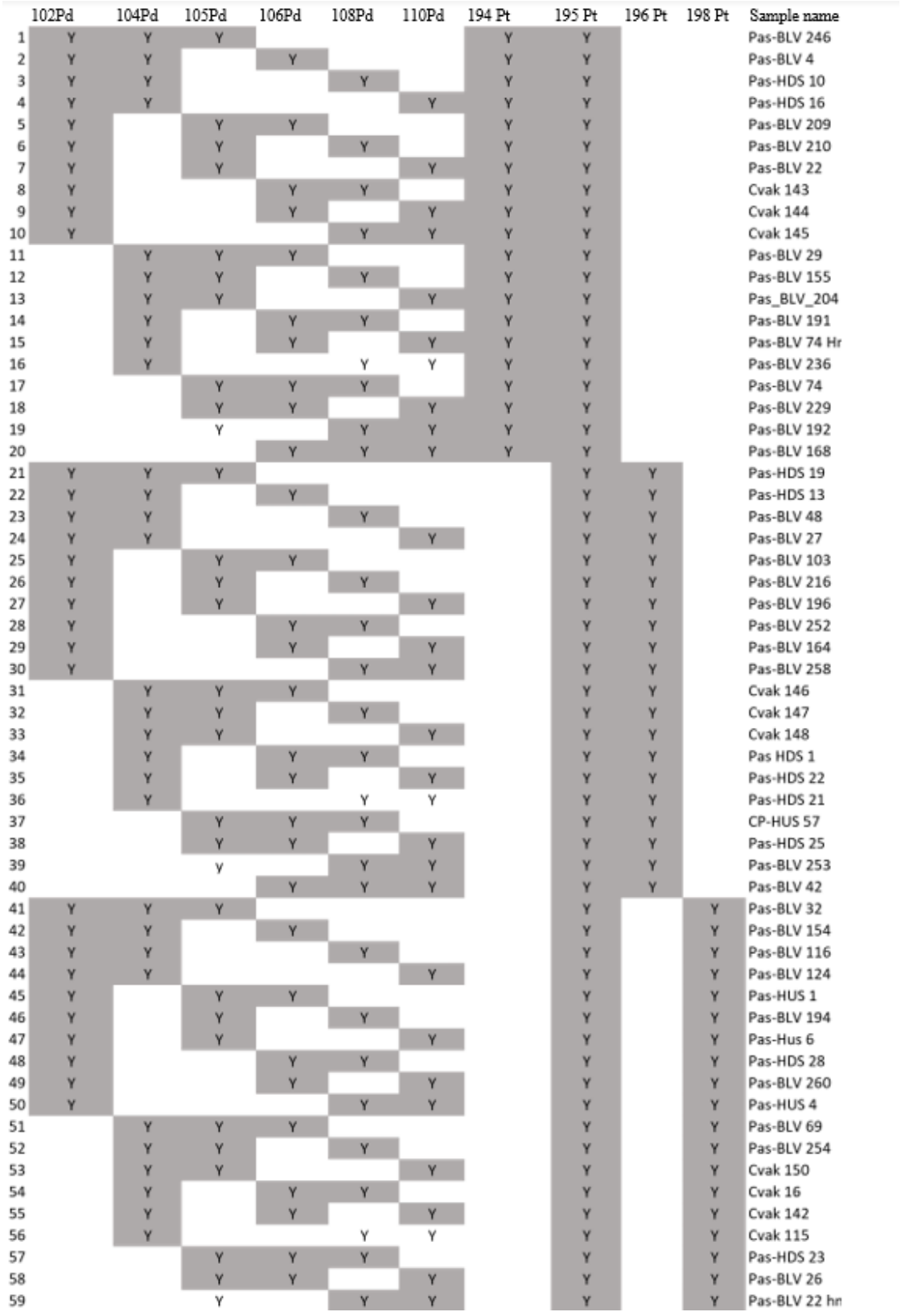

	102Pd	104Pd	105Pd	106Pd	108Pd	110Pd	194 Pt	195 Pt	196 Pt	198 Pt	Sample name
1	Y	Y	Y				Y	Y			Pas-BLV 246
2	Y	Y		Y			Y	Y			Pas-BLV 4
3	Y	Y			Y		Y	Y			Pas-HDS 10
4	Y	Y				Y	Y	Y			Pas-HDS 16
5	Y		Y	Y			Y	Y			Pas-BLV 209
6	Y		Y		Y		Y	Y			Pas-BLV 210
7	Y		Y			Y	Y	Y			Pas-BLV 22
8	Y			Y	Y		Y	Y			Cvak 143
9	Y			Y		Y	Y	Y			Cvak 144
10	Y				Y	Y	Y	Y			Cvak 145
11		Y	Y	Y			Y	Y			Pas-BLV 29
12		Y	Y		Y		Y	Y			Pas-BLV 155
13		Y	Y			Y	Y	Y			Pas_BLV_204
14		Y		Y	Y		Y	Y			Pas-BLV 191
15		Y		Y		Y	Y	Y			Pas-BLV 74 Hr
16		Y			Y	Y	Y	Y			Pas-BLV 236
17			Y	Y	Y		Y	Y			Pas-BLV 74
18			Y	Y		Y	Y	Y			Pas-BLV 229
19			Y		Y	Y	Y	Y			Pas-BLV 192
20				Y	Y	Y	Y	Y			Pas-BLV 168
21	Y	Y	Y					Y	Y		Pas-HDS 19
22	Y	Y		Y				Y	Y		Pas-HDS 13
23	Y	Y			Y			Y	Y		Pas-BLV 48
24	Y	Y				Y		Y	Y		Pas-BLV 27
25	Y		Y	Y				Y	Y		Pas-BLV 103
26	Y		Y		Y			Y	Y		Pas-BLV 216
27	Y		Y			Y		Y	Y		Pas-BLV 196
28	Y			Y	Y			Y	Y		Pas-BLV 252
29	Y			Y		Y		Y	Y		Pas-BLV 164
30	Y				Y	Y		Y	Y		Pas-BLV 258
31		Y	Y	Y				Y	Y		Cvak 146
32		Y	Y		Y			Y	Y		Cvak 147
33		Y	Y			Y		Y	Y		Cvak 148
34		Y		Y	Y			Y	Y		Pas HDS 1
35		Y		Y		Y		Y	Y		Pas-HDS 22
36		Y			Y	Y		Y	Y		Pas-HDS 21
37			Y	Y	Y			Y	Y		CP-HUS 57
38			Y	Y		Y		Y	Y		Pas-HDS 25
39			Y		Y	Y		Y	Y		Pas-BLV 253
40				Y	Y	Y		Y	Y		Pas-BLV 42
41	Y	Y	Y					Y		Y	Pas-BLV 32
42	Y	Y		Y				Y		Y	Pas-BLV 154
43	Y	Y			Y			Y		Y	Pas-BLV 116
44	Y	Y				Y		Y		Y	Pas-BLV 124
45	Y		Y	Y				Y		Y	Pas-HUS 1
46	Y		Y		Y			Y		Y	Pas-BLV 194
47	Y		Y			Y		Y		Y	Pas-Hus 6
48	Y			Y	Y			Y		Y	Pas-HDS 28
49	Y			Y		Y		Y		Y	Pas-BLV 260
50	Y				Y	Y		Y		Y	Pas-HUS 4
51		Y	Y	Y				Y		Y	Pas-BLV 69
52		Y	Y		Y			Y		Y	Pas-BLV 254
53		Y	Y			Y		Y		Y	Cvak 150
54		Y		Y	Y			Y		Y	Cvak 16
55		Y		Y		Y		Y		Y	Cvak 142
56		Y			Y	Y		Y		Y	Cvak 115
57			Y	Y	Y			Y		Y	Pas-HDS 23
58			Y	Y		Y		Y		Y	Pas-BLV 26
59			Y		Y	Y		Y		Y	Pas-BLV 22 hr

Figure 7 Schematic presentation of the barcoding patterns. *Each sample gets stained with three different palladium isotopes and two cisplatin.*

2.1.2.2.1 Sample barcoding

Barcode mix with 20 plex barcode and both cisplatin isotopes were prepared in a 96 well rack. Cisplatin isotopes used was pre-optimized by Flow Cytometry Core Facility at University of Bergen, Resulting in the appropriate volume of 200nM cisplatin of each isotope for each sample. Each sample contained 7 µl of 20 plex palladium barode and 4 µl of each cisplatin.

Fixed cells were rapidly thawed, washed with MaxPar^{TM} CBS (Fluidigm Corporations, South San Fransisco, California, US), and transferred to a 96 well plate with 100µl MaxPar^{TM} PBS. Before adding the barcode reagent, cells were washed twice with 200µl MaxPar^{TM} 1X Barcode Perm buffer mixed (10X barcode perm buffer mixed with Maxpar® PBS in the ratio 1:9). Barcode perm buffer is essential for CyTOF® signal-to-noise detection. Centrifugation conditions were 500g for 5 min at 20^{o}C. All centrifugation in the barcoding stage was done with these conditions if nothing else is mentioned.

After last wash, cells are resuspended in 100µl barcode perm buffer. Approximately 85 µl barcode perm buffer was added to barcode mix giving a total volume of 200µl. Cell suspension and barcode was mixed immediately and incubated for 30 minutes at room temperature on a shaker (300rpm). At 5 and 10 minutes, the cells were mixed by pipetting. All samples were washed with 250µl Maxpar® CBS five times, before being resuspended in 100 µl Maxpar® CBS and incubated on ice. To verify that all barcode quality, 5 µl of each well were mixed into 3 tubes (one tube per 20 plex barcode) and acquired on the CyTOF. After verifying that the barcodes could be debarcoded appropriately, all barcodes were transferred into 3 tubes according to the 20 plex barcode and stored at -80^{o}C.

2.1.2.3 Antibody staining of barcoded samples

Before staining the barcoded samples, cells were washed once with 9 mL Maxpar® CSB and counted using Bürker hemocytometer. For each of the three barcoded samples (20 samples in each barcode), it was counted 15 million, 11 million, and 17,8 million cells. Barcoding protocol suggests that the number of cells in each sample ideally should be 1-3 million, whereas in this study lower number of cells per samoles were estimated to 0.6-0.9 million.

Samples were washed with Maxpar® CBS and the cell pellet was transferred to a FACS tube. Already aliquoted 3µl heparin solution (100IU/ml) was added into the tube and incubated on shaker for 15 minutes. 90 µl of premade antibody cocktail with some adjustment with IgA

(chapter 2.12.3) was added to the sample and incubated for 30 minutes. After 30 minutes the sample was washed twice with 3mL Maxpar® CSB.

Fresh paraformaldehyde (PFA) and perm buffer is added to thoroughly fix the cell and also the antibodies to the cells. In addition, per ensures the access and binding of Iridium (Ir) to the cellular nucleic acid. Fix and perm buffer was diluted with 0.1 nM Iridium-nucleic acid intercalator (Fluidigm) and 4% PFA (Alfa Aesar, 16% PFA, methanol-free) containing Maxpar^{TM} PBS. Samples were stored overnight at 4^{o}C.

Right before acquiring on the CyTOF, cells were washed once with Maxpar^{TM} CBS and twice with Maxpar^{TM} CAS and resuspended in Maxpar^{TM} CAS supplemented with 1:10 dilution of EQ Four Element Calibration beads at a cell concentration of >1.0 million cells pr milliliter.

2.1.2.4 Antibody titration

Antibody titration is used for determining the optimal concentration of antibodies. The right concentration of antibodies is crucial since low concentrations lead to poor antibody-cell ratio and high concentrations can lead to high background or false-negative results. If the panel consists of high concentration of one antibody it will bind with low affinity to cells and will not replicate and show a correct image of the immunological aspects in the samples.

For antibody titration, PBMC were used. Thawed PBMC were washed with Maxpar® Cell staining buffer twice. Heparin was added to the cells and incubated for 10 min before in-house and premade 11 antibody backbone panel covering the main populations of the immune system (CD3, CD4, Cd8, CD11c, CD14, CD16, CD19, CD45, CD56, CD66b, HLA-DR) was added and incubated for 30 minutes. While incubation, the antibody for titration was made ready. Six eppendorf tubes were marked and filled with 20µl Maxpar® CSB, except in the first Eppendorf tube which had 40 µl added. To the first tube 2µl antibody was added, and from this tube 20µl were transferred to tube 2, mixed carefully and from this 20µl were transferred into tube 3 etc. From the last tube, after mixing, the 20µl was discarded. All cells stained with backbone, were equally divided and added to the tubes and acquired individually. This resulted in the concentrations 1/100, 1/200, 1/400, 1/800, 1/1600, and 1/3200.

Data was analyzed in Cytobank^{TM} and the staining index was calculated. Stain index is calculated with the difference between the positive and negative population of the antibody titrated, divided on the standard deviation of the negative population times two

(equation 3.1.4). Higher staining index with low background noise means good antibody concentration (53). Values from this study are given in table 2 and figure 8.

$$staining\ index\ (\Delta) = \frac{MFI_{pos} - MFI_{neg}}{2\ x\ SD} \quad (3.1.4)$$

Table 2 Overview of the dilutions and their negative population median, positive population median, standard deviation and staining index.

Dilution	Negative population median	Positive population median	Standard deviation	Stain index
1/100	2.62	84.83	4.73	8.69
1/200	1.56	68.72	3.90	6.63
1/400	0	15.64	1.65	4.75
1/800	0	17.27	1.70	5.09
1/1600	0	7.84	1.11	3.57
1/3200	0	8.16	1,11	3.68

In table 2 the median and standard deviation values for negative and positive populations are taken from Cytobank after gating of the populations. Staining index is calculated manually using equation 3.1.

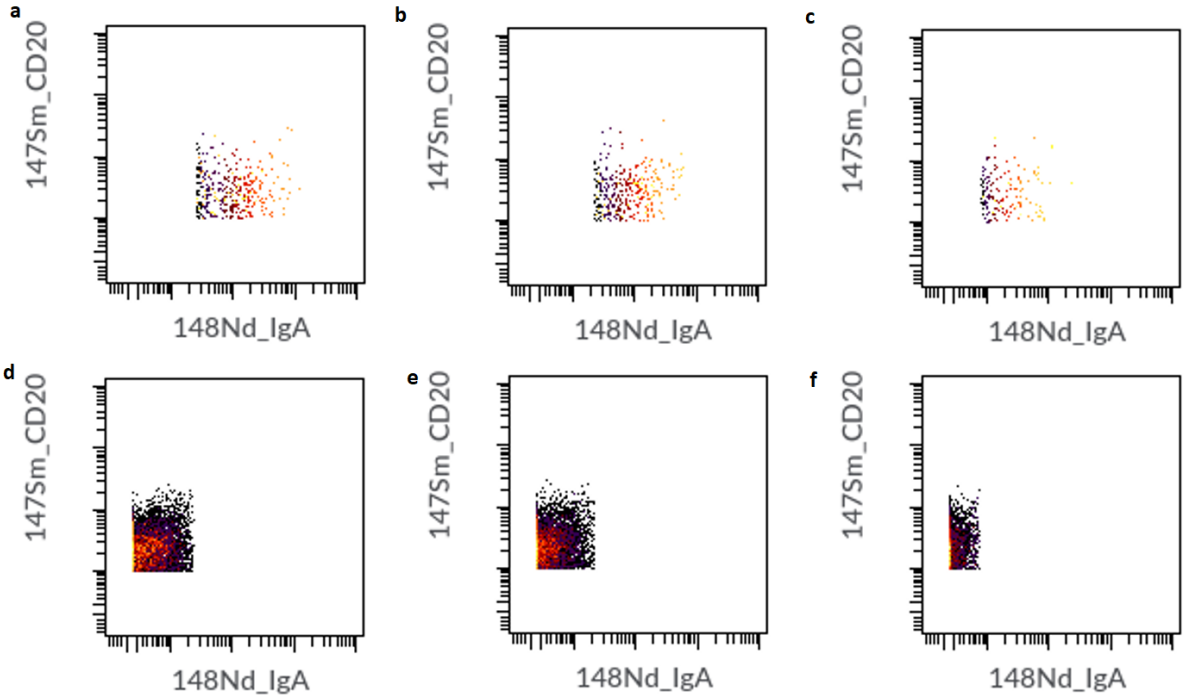

Figure 8 Positive and negative populations of the titrated IgA. *Figure a-c shows the positive population of IgA with different concentrations. Figure d-f shows the negative population of IgA with different concentrations. Figure a and d shows 1:100 titers, figure b and e show 1:200 titers and figure c and f show 1:400 titers. Plots adapted from Cytobank.*

2.1.2.5 Calibration Beads

EQTM Four Element Calibration Beads (containing 140/142Ce, 151/153Eu, 165Ho, and 175/176Lu) were used for identifying and monitoring instrument differences and fluctuation across batches and during data acquisition. The beads are used to correct for inter-sample variations and intra-sample variations.

2.1.4 Data analysis

Manual gating on biaxial plots in mass cytometry involves a high error risk, time-consuming, susceptible to operator bias, and not easily scalable (54). Computational challenges such as pre-processing, normalization, dimensional reduction, and clustering can arise while analyzing high-dimensional single-cell data. However, traditional approaches are mastered with advanced algorithms that fundamentally altering the processing and interpretation of the data. Although algorithms, such as SPADE, FlowSOM, and tSNE are available through Cytobank®, a large number of choice and lack of consensus on the best data for pre-processing and analysis is problematic (55). SPADE and FlowSOM are clustering algorithms that group cell populations together based on the expressed markers. tSNE algorithms aim to give an easier visualization by presenting single-cell data in a two-dimensional map (56). In this project the cluster

annotation, identification of subpopulations, and statistical analysis was done by cloud-based cytometry analysis platform, Astrolabe Diagnostics located in New Jersey, USA. Astrolabe provides labeling of the cells with Ek'Balam hierarchy-based algorithm. This algorithm combines knowledge-based gating strategy with unbiased FlowSOME R package clustering (56). Statistical analyses were performed using Astrolabe Diagnostics. False discovery rate (FDR) adjusted $p \leq 0.05$ and above were considered statistically significant.

Identifying cell subtypes/populations that differed in the different study participants volcano plots were used. Volcano plots show the spread of populations on the x-axis and the confidential interval on the y-axis. Subpopulations that differ within the study group have a higher y-axis value and thereby higher significance. However, using this method must be doublechecked, since some subsets can be strongly expressed that it will give a biased result for the whole parent population.

2.2 Specific aim 2

2.2.1 Materials

19 substances were received from professor Torgils Fossen, University of Bergen. Out of these 19 substances, four substances were chosen for MTT assay; Ellagic acid (EA), Rumic acid, Plantainoside D, and Dinatin 7-glucuronide. These compounds were tested on three different cell lines for cytotoxic concentration identification. Human embryonic kidney cells (HEK293, ATCC), human embryonic kidney cells variant that express a temperature- sensitive allele of SV40 T antigen (HEK-293t, ATCC), and colorectal adenocarcinoma cells 2 (CACO-2, ATCC) has been selected to be used in this project. These three different adherent cell lines replicate the epithelial cells located in different places in the body, where two of these have a positive replication of SARS-CoV-2 virus and one has negative replication.

2.2.2 Methods

2.2.2.1 Cell culturing

HEK293 (ATCC) and HEK293t (ATCC) were cultured in Gibco™ Dulbeccos Modified Eagles's Medium (DMEM,) with high glucose and 2mM Glutamine, supplemented with 10% Fetal Bovine Serum (FBS). CACO-2 (ATCC) were cultured in Gibco™ DMEM supplemented with 10% FBS and 1% Gibco™ MEM non-essential amino acids.

Cell lines were kept in cell tissue incubators at 37 °C and 100% humidity with 95% air and 5% CO_2 cultured in 75 cm^2 culture flasks (Nunc, Thermo Fischer Scientific, Waltham, Massachusetts, USA) in monolayers. Cell culturing happened under sterile conditions.

2.2.2.2 Passaging, seeding, expanding, and cryopreservation of cells

Sub-culturing, seeding, expanding, cryopreservation, and thawing of the cells was done according to ATCC® protocol for HEK293 and HEK293t cell lines. While the same procedures as described in the product sheet for CACO-2 were followed. Cells were used between passage 5 to 17.

Sub-culturing of the cells was done by removing the growth medium with a pipette. Cells were washed with phosphate buffered saline (PBS, Ficher Scientific, Arendalsvagen, Goteborg, Sweden) and loosened with Trypsin EDTA at 37°C for 2-3 minutes. Growth medium was used for resuspending the cells and appropriate dilution of cells was transferred in a new flask with more growth medium added.

In the ATCC® protocol for CACO-2 cells, Eagle's minimum essential medium (EMEM) is recommended to be used. However, the growth medium was changed to Gibco™ Dulbecco's Modified Eagle Medium (DMEM) supplemented with 10% FBS and 1% Gibco™ MEM non-essential amino acids, because of the lack of availability of EMEM.

2.2.2.3 MTT (3-(4, 5-dimethylthiazolyl-2)-2, 5-diphenyltetrazolium bromide) assay

MTT (3-(4, 5-dimethylthiazolyl-2)-2, 5-diphenyltetrazolium bromide) assays is a non-radioactive method used for quantification of cell proliferation and viability of cells. This assay is established on the yellow tetrazolium salt MTT metabolization. Metabolic active cells cleave MTT with pyridine nucleotide cofactors NADH and NADPH from the viable cells, resulting in purple formazan crystals as shown in figure 9. Formazan crystals are insoluble, but with the help of a solubilization solution, the crystals are dissolved resulting in a solution that is colored. Absorbance of the colored solution is measured with a multi-well spectrophotometer. Lighter solutions contain less viable metabolically active cells. (57)
Downside with using this method is the lack of sensitivity compared using fluorescent and luminescent methods. However, the sensitivity is dependent on the cell types that are being tested. Along with the lack of the sensitivity, chemical compounds can increase the background absorbance values resulting in artifacts. One example of these compounds is ascorbic acid and

vitamin A. If the MTT assay is exposed to light and high pH too long the background noise might get elevated.

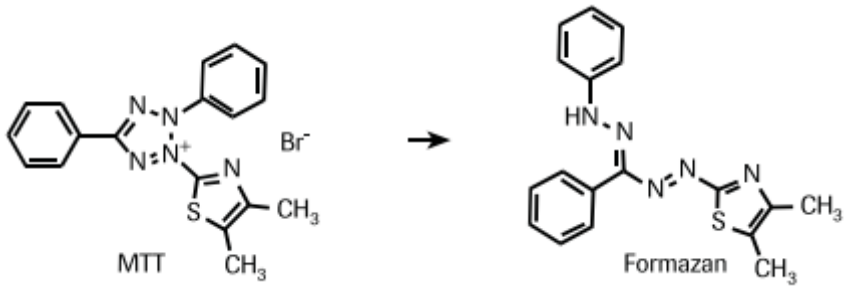

Figure 9 Overview of metabolic active cells cleavage of MTT to formazan crystal. *Figure adapted from (57). Reprinted with permission from Springer/Rightslink*

2.2.2.3.1 Substances tested with MTT assay

Ellagic acid (EA) is a compound that is extracted from different fruits and vegetables, such as raspberries, strawberries, cranberries, and pomegranates. This compound is undergoing clinical trials for the treatment of Follicular Lymphoma, cardiovascular functional improvement in obese younger adults/adolescents, solar lentigines treatment, and protect intrauterine growth restricted babies from brain injury. Mainly, the effect is believed to be in their antioxidant and anti-proliferative properties (58, 59)

In previous studies, it has been shown that EA affects immunological activities by regulating different proinflammatory cytokines, such as IL-6, IL-1β, and TNF-α. It has also been shown that it affects NF-κβ. Continuously exposure to TNF-α can lead to inflammation local and systematic (58). In one study it was shown that TNFα mediated production of IL-6 and IL-8 waws inhibited by EA.

Rumic acid (RA) used in this project was extracted from *Peucedanum ostruthium* and belongs to the flavonoids group that is associated with biochemical and pharmacological effects, such as antioxidative, anticarcinogenic, anti-inflammatory, and antiviral properties. Anti-inflammatory responses include targeting cyclooxygenase and cytokines, such as TNF-α. (60)

Plantainoside D (PD) is an antioxidative compound that was extracted from *Plantago major* and has been used in treating diseases that are associated with free radicals. For example, in treatment with the anti-tumor drug, Adriamycin, plantainoside D has shown to have inhibiting effects on the ROS generation and NF-kB activation and thereby preventing apoptosis of the cardiac muscle cells (61).

Dinatin 7-glucuronide (D7G) is a flavone that is found in the leaves of *Plantago major*. Plantago major has different pharmacological activities, such as analgesic, antibacterial, antidiarrheal, anti-inflammatory, antioxidant, antiviral, immunomodulatory, and immunostimulatory. The different pharmacological activities might depend on which part of *Plantago major* is being used. (62)

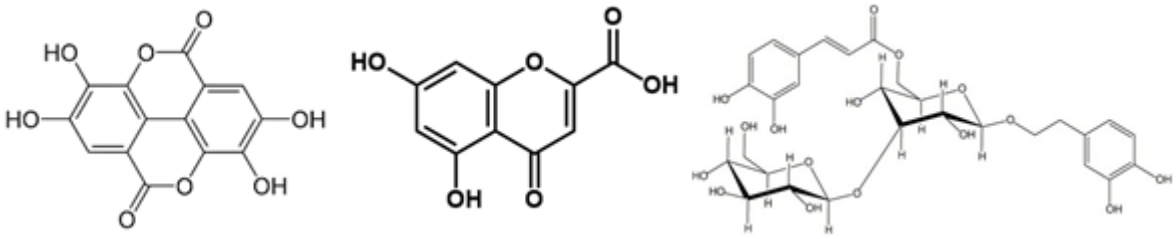

Figure 10 Chemical structure for Ellagic acid, rumic acid and plantainoside D. Chemical structures were made in ChemDraw

2.2.2.3.2 MTT preparation

Optimal concentrations of the stock solution required dilution of the stock solutions (Table 3). Further dilution was done with the DMSO (Sigma Aldrich Norway AS, Oslo). EA and RA concentrations at 10mM, 1 mM, 100 µM, 10µM, 1µM, 100nM, 10nM and 1 nM was tested. For D7G and PD 1 mM, 100 µM, 10µM, 1µM, 100nM, 10nM and 1nM was tested. For D7G one additional concentration at 0.1nM was tested. Dilution method and overview of concentrations for each compound is further described in figure 11 and 12.

Table 3 Amount and concentrations received from Torgils Fossen and amount used for making the concentration needed for each compound

	Concentration on received raw material	DMSO (µL)	Concentration (mM)
Ellagic acid	33,5 mg	1100	100
Rumic acid	2916 mM	96,6	100
Dinatin 7-glucuronide	11,9 mM	16	10
Planainoside D	780 mM	84	10

EA was received as solid, while the rest of the compounds were liquids.

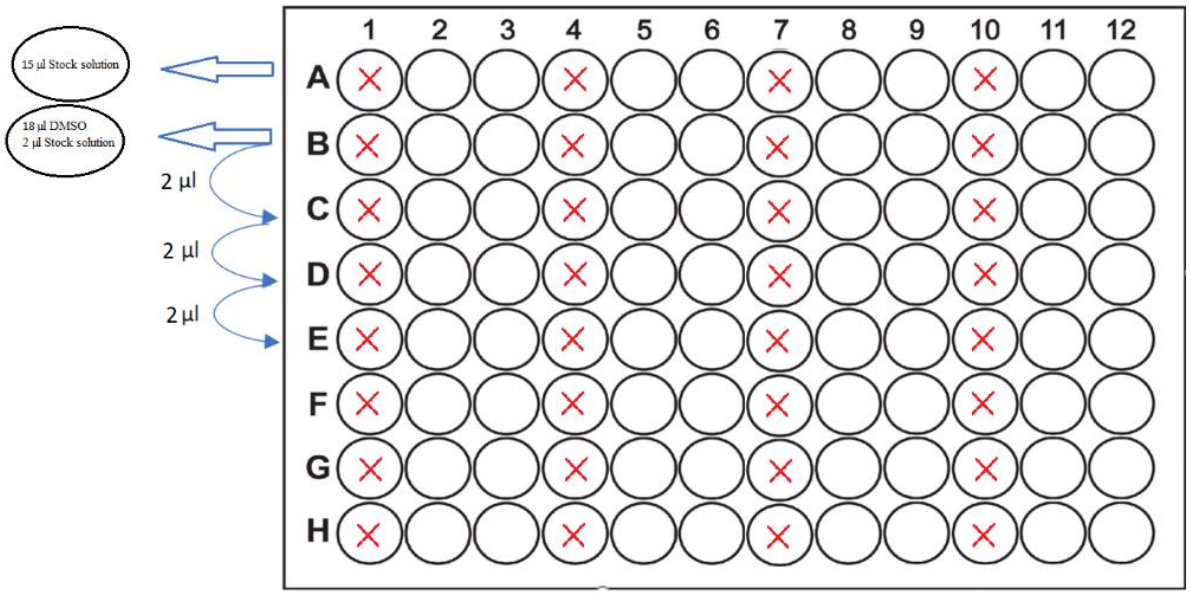

Figure 11 Overview of the setup for making dilutions solutions in a 96 well plate. *15µl each stock volume was transferred to A wells (as marked in the figure). In B wells 18µl DMSO and 2µl stock volume were added to C well and so on.*

Solution made as shown in figure 11 was directly transferred to 96 well plate with 3 x 10^4 cells in each well, so the end concentration ended up as shown in figure 12.

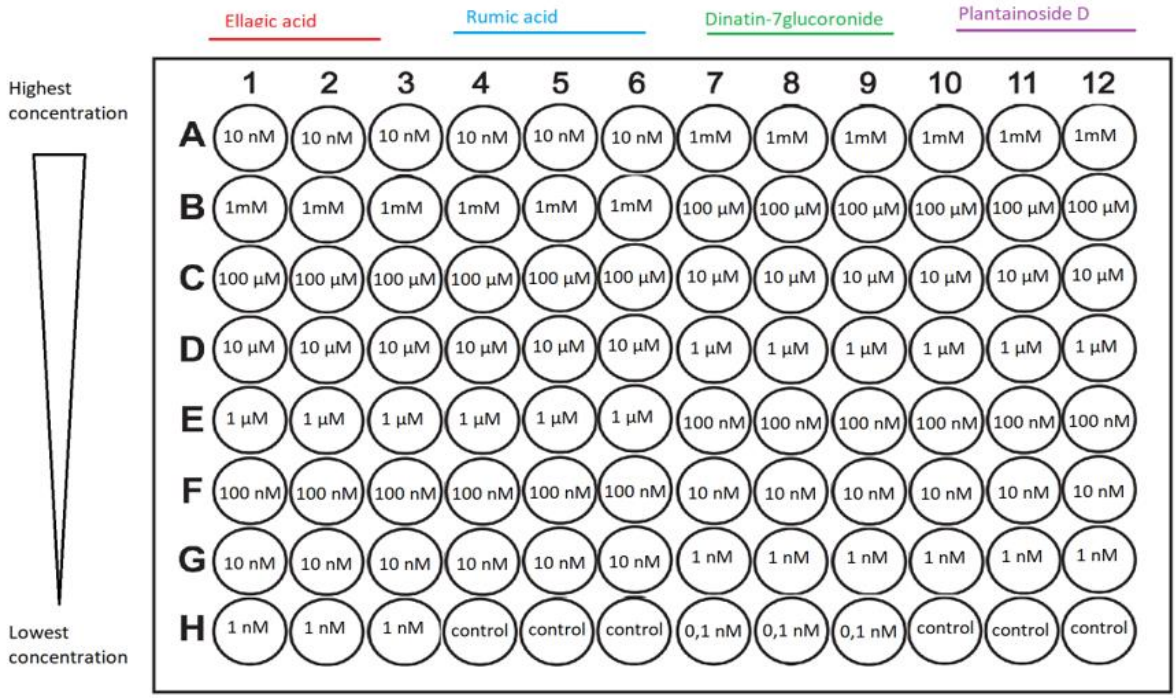

Figure 12 Overview of the setup for each compound concentration in the 96 well plate.

3 x 10^4 cells per well for the three cell lines were exposed for different concentrations of the compounds as described in figure 12. Cells was incubated for 24 hours in incubator at 37°C and

5% CO_2. After 24 hours 10 µl of MTT labeling agent (Sigma, St Louis, MO, USA)) and incubated for 4 hours before adding 100 µl solubilization solution (10% Sodium dodecyl sulfate solution in 0.1M HCl, Sigma, St Louis, MO, USA) overnight in incubator at 37ºC and 5% CO_2, before measuring the spectrophotometrical absorbance in Synergy™ H1 microplate reader (BioTek instruments Winooski, VT, USA).

2.3 Instruments used in this project

Mass cytometer: Fluidigm CyTOF Helios™ analyzer (Fluidigm Corporation, South San Francisco, California, USA) was used for defining metal properties of cells.

Cell counting: Bürker Haemocytometer counting chambers (Sigma Aldrich, MilliporSigma, Missouri, USA) was used to count cells before staining antibodies, running samples on the CyTOF, and to count HEK293, HEK293t, and CACO-2 cells.

Centrifuge: Centrifuge 5810 R (Eppendorf, Hamburg, Germany) was used for centrifugation of samples in the lysis process and of 96 well plates.

Eppendorf centrifuge: Eppendorf Centrifuge 5417 C (Eppendorf, Hamburg, Germany) was used for spinning down cell pellets while staining and barcoding samples.

Cell culture imaging: Cytation 5 Cell Imaging multi-mode reader (Biotek instrument Inc, Winooski, USA) was used for imaging 96 well plate with cell cultures for determining ideal concentrations.

96 well microplate reader: Biotek Synergy H1 Hybrid multi-mode microplate reader (BioTek instruments Winooski, VT, USA) was used for measuring the spectrophotometric absorbance of the samples in the MTT project.

2.4 Software used in this projects

Word: the project has been written and edited on Microsoft ® Word for Microsoft 365 MSO (Microsoft Corporation, Redmond, Washington, USA)

Excel: Histograms and graphs were made with Microsoft ® Excel for Microsoft 365 MSO (Microsoft Corporation, Redmond, Washington, USA)

Mass cytometry analysis software: Analysis of high parameter workflows was done in Cytobank Inc., (Beckman Coulter Life Science. Indianapolis, USA).

Astrolabe Diagnostics; Paid service from Astrolabe diagnostics (Fort Lee, NJ, USA) was used for analyzing mass cytometric data.

3. Results

3.1 Specific aim 1

Mass cytometry with a pre-made antibody panel (Supplementary) was used to immunophenotype different peripheral blood cell subsets from patients who had been infected with SARS-CoV-2 six months prior to the analysis and healthy controls. In this study, major immunological subtypes in SARS-CoV-2 infected patients and healthy controls were investigated (Table 4). Total cell count below 20 000 cells was considered low, and 4 patients with mild disease, 2 patients with severe disease, and 1 healthy control came under this category but included in further analysis.

Table 4 Immune cell subtypes identified by the Astrolabe Cytometry Platform

Population names	Surface receptors
B cells	CD3- CD14- CD19+ CD56-CD66b -
B naïve	CD24- CD27-
B memory	CD27+ CD38-
Switched memory	IgD-
Non-switched memory	IgD+
Plasmablast	CD20- CD27+ CD38+
Transitional	CD38+ CD24+ CD27+
T cells	CD3+ CD14- CD19- CD56-
Double negative	CD4- CD8- TCRgd-
Double positive	CD4+CD8+ TCRgd-
CD4+	CD4+ CD8-
Naïve	CD45RA+, CD27+
Central memory	CD45RA-, CD27+
Effector memory	CD45RA-, CD27-
CD4+Tregs	CD25+ CD127-
CD8+	CD4- CD8+ TCRgd-
Naïve	CD45RA+ CD27+
Central memory	CD45RA- CD27+
Effector memory	CD45RA- CD27-
Gamma delta T cells	TCRgd+
NK cells	CD3- CD14- CD19- CD56+ CD66b -
Natural killer (CD56+ CD16+)	CD16+
Natural killer (CD56+ CD16-)	CD16-
NKT cells	CD3+ CD14- CD19- CD56+ CD66b -
Dendritic cells	CD3- CD14- CD19- CD56- CD66b-
Conventional dendritic cells type 1	CD123- HLA_DR+, CD16- CD141+
Plasmacytoid dendritic cells	CD11c- CD123+ HLA_DR+
Monocytes	CD3- CD14+ CD19- CD66b-
Classical	CD14+ CD16+
Intermediate	CD14+ CD16-
Non-classical	CD14- CD123- HLA_DR+, CD16+ CD141-
Granulocytes	CD3- CD14- CD19- CD56- CD66b+
Basophils	CD123+ HLA_DR-

Main population in bold. Subpopulations indicated with additional receptors for identification

3.1.1 SARS-CoV-2 patients and healthy controls display similar frequencies of whole blood cell populations

Varies cell subset frequency differences amongst healthy controls and SARS-CoV-2 infected recovered patients were observed. However, in parent/main populations no significant variations in cell frequencies were found. Small differences in cell frequencies were observed in the T cell population and granulocytes (figure 13). Compared to the healthy controls, patients had a slightly higher frequency (FDR = 0.095) in overall T cells 6 months post-infection, while granulocytes had a small decrease in the patient group (FDR=0.057)

Astrolabe Diagnostics uses a multidimensional clustering algorithm and assign all cluster into known subsets based on markers used by the algorithm (figure 14). Astrolabe found known subset and unassigned subpopulations. In figure 14, figure 15, and figure 16, some subsets in the myeloid and T cells show higher fold change than other subsets.

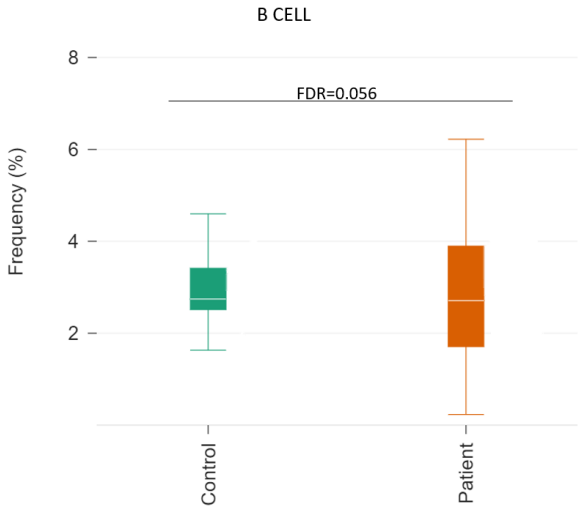
B CELL
FDR=0.056
Frequency (%)
8
6
4
2
Control
Patient

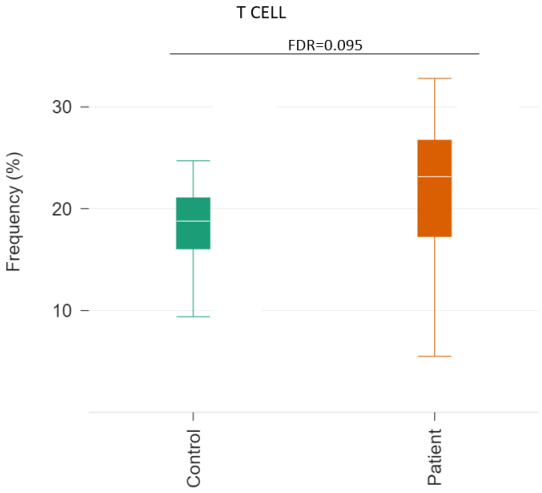
T CELL
FDR=0.095
Frequency (%)
30
20
10
Control
Patient

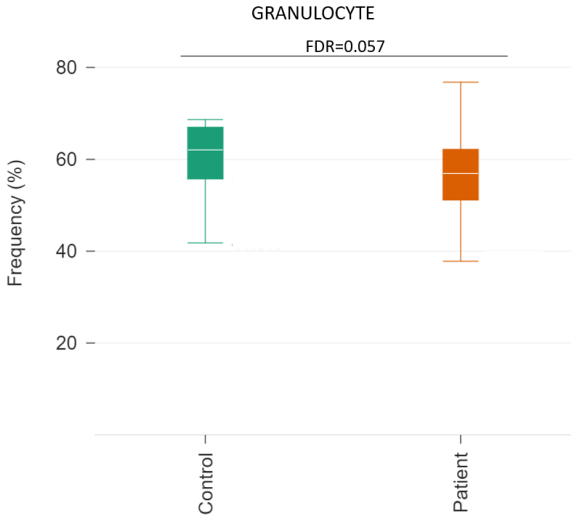
GRANULOCYTE
FDR=0.057
Frequency (%)
80
60
40
20
Control
Patient

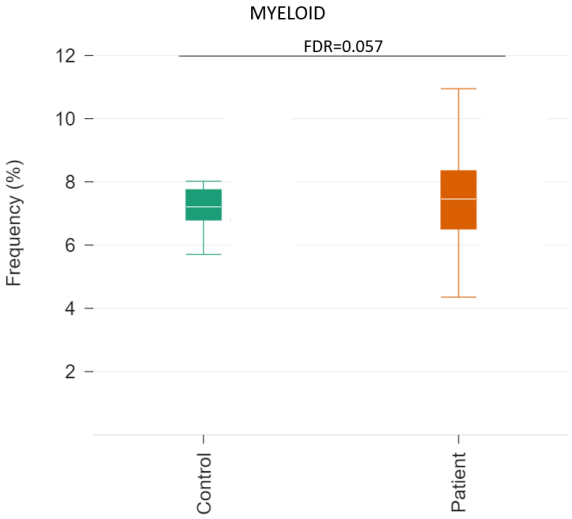
MYELOID
FDR=0.057
Frequency (%)
12
10
8
6
4
2
Control
Patient

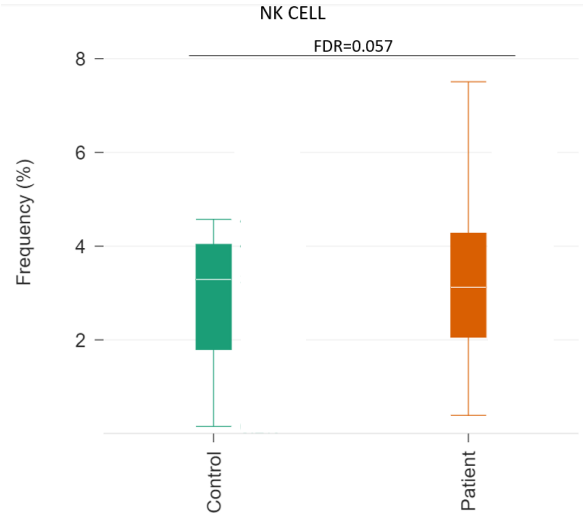
NK CELL
FDR=0.057
Frequency (%)
8
6
4
2
Control
Patient

Figure 13 Overview of compartment populations in SARS-CoV-2 patients and healthy controls. *Comparisons were made among healthy controls (n=10) and SARS-CoV-2 infected patients (n=49). Single-cell data was clustered together with FlowSOME R package with Ek'Balam algorithm labeling. Median for each cell population is stated and statistical significance is considered with FDR/adjusted for 0.05 ≥ p.*

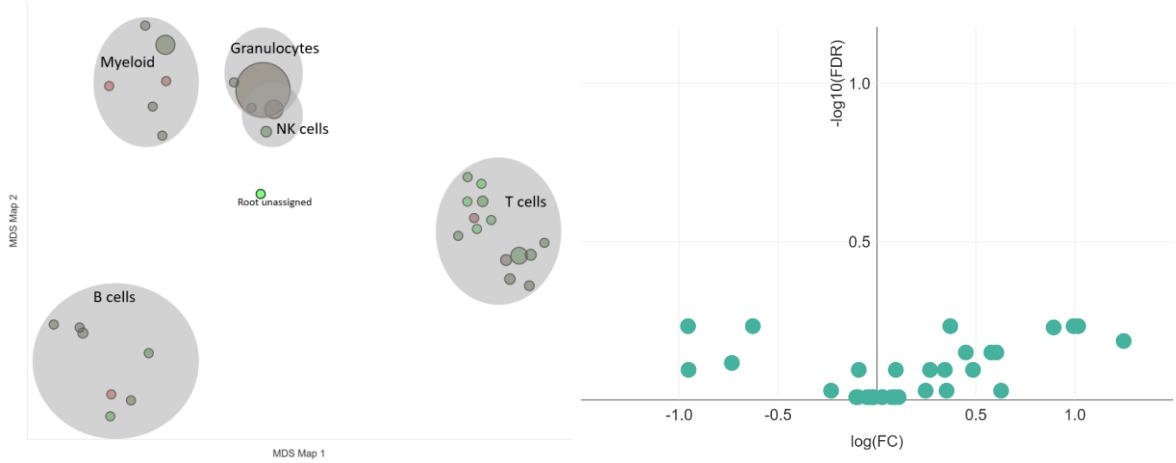

Figure 14 Differential abundance analysis amongst healthy controls(n=10) and SARS-CoV-2 patients (n=49). *a) Cell subsets overview in a multidimensional scaling map (MDS) found by Astrolabe Diagnostics using labeling Ek'Balam algorithm (Amir et. al., 2019 (56)) and clustered together with FlowSOM R package (Van Gassen et. al 2015(63)). b) Frequency across all assigned subsets in a volcano plot. False discovery rate (FDR), Fold change (FC).*

Exploring subcellular populations of T-cells, B cells, myeloid, and granulocytes, difference was found in 5 populations. Although, $CD4^+$ central memory T cells (Figure 15A) were increased in the patient group (FDR = 0.233), large spread in the data is shown. In contrast, no differences were seen in $CD8^+$ T central memory cell frequencies (Figure 15B).

Figure 16 shows a small median frequencies value and spread in the γδ T cells for the two groups. However, two samples in the control group showed very low frequencies of γδ T cell population, while one patient sample had relatively high frequency.

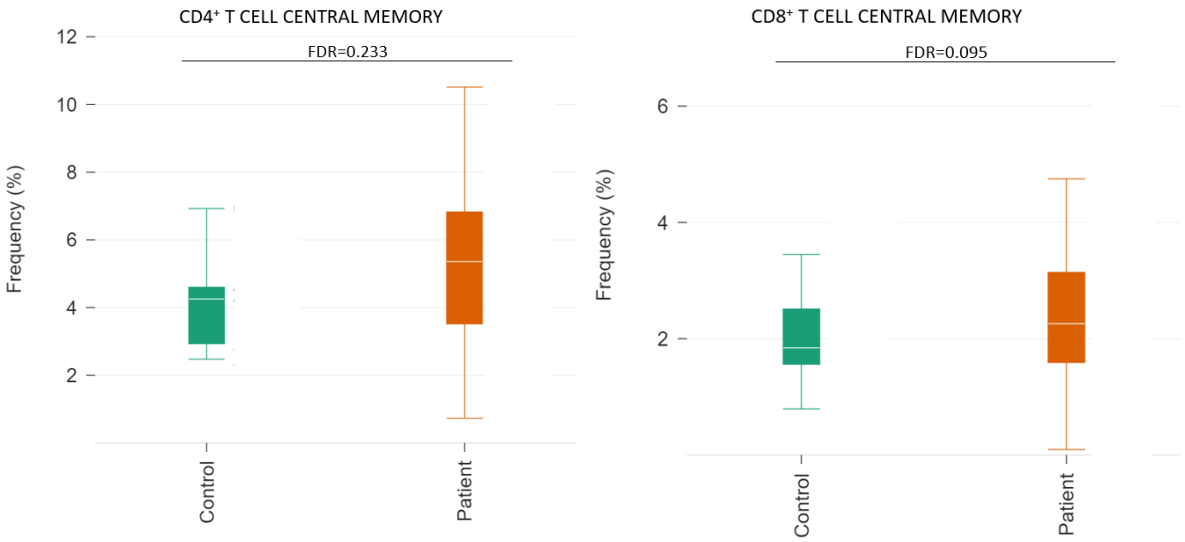

Figure 15 T cell subpopulations *A) CD4$^+$ central memory T cells frequencies in healthy controls (n=10) and SARS-CoV-2 patients (n=49). FDR=0.233. B) CD8$^+$ central memory T cell frequencies in healthy controls (n=10) and SARS-CoV-2 patients (n=49). FDR=0.095. Single-cell data was clustered together with FlowSOME R package with Ek'Balam algorithm labeling. Median for each cell population is stated and statistical significance is considered with FDR/adjusted for 0.05 ≥ p.*

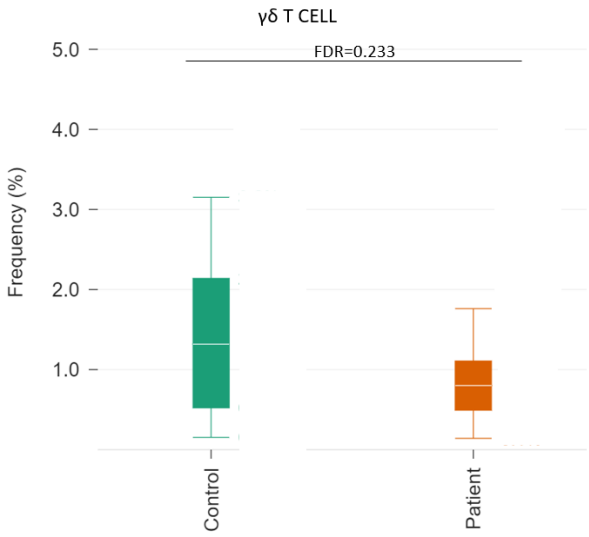

Figure 16 γδ T cell frequencies in control samples (n=10) versus patient samples (n=49). *FDR=0.233. Single-cell data was clustered together with FlowSOME R package with Ek'Balam algorithm labeling. Median for each cell population is stated and statistical significance is considered with FDR/adjusted for 0.05 ≥ p.*

Looking into the monocyte compartment, two subpopulations showed differences (figure 17). The classical monocytes show significantly higher frequency (FDR=0.095) in the patient group compared to healthy controls (figure 17a). Four SARS-CoV-2 infected patients had ≥ 0.6% frequencies of CD14- CD16+ non-classical monocytes (figure 17b), resulting in a high negative impact on the overall result for this small population of non-classical monocytes. No significant differences for dendritic cell type 1 were observed (figure 18), but the median differs in the two groups. 3 out of 10 healthy control samples showed a very low frequency <0,05 % dendritic cell type 1 frequencies, and 1 of the patient sample had 0.45% frequency.

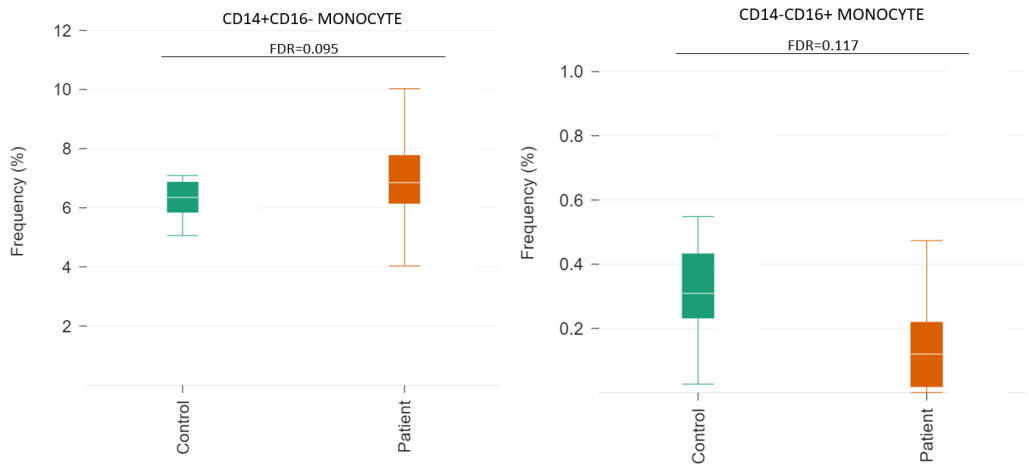

Figure 17 Myeloid compartments. *A) CD14+ CD16- classical monocyte frequencies in patient (n=49) and healthy controls (n=10). FDR= 0.095. B) CD14- CD16+ non-classical monocyte frequencies in patient (n=49) and healthy controls (n=10). FDR= 0.117. Single-cell data was clustered together with FlowSOME R package with Ek'Balam algorithm labeling. Median for each cell population is stated and statistical significance is considered with FDR/adjusted for 0.05 ≥ p.*

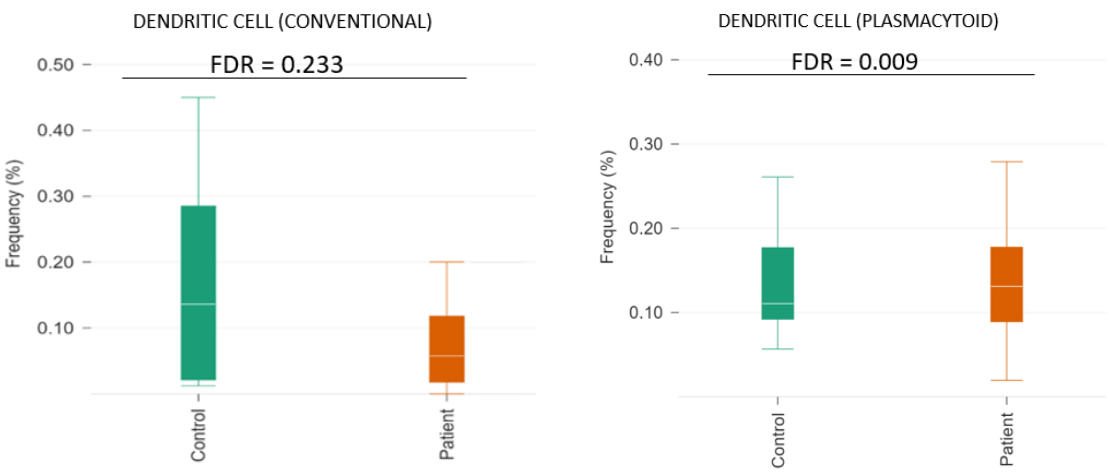

Figure 18 Dendritic cell frequencies in patients and healthy controls. *A) Dendritic cell type 1, CD141$^+$ cell frequencies in controls (n=10) and patients (n=49). FDR=0.233. B) Plasmacytoid dendritic cells in healthy controls (n=10) and patients (n=49). FDR=0.009 Single-cell data was clustered together with FlowSOME R package with Ek'Balam algorithm labeling. Median for each cell population is stated and statistical significance is considered with FDR/adjusted for 0.05 ≥ p.*

3.1.2 Moderate and severe patients showed altered expressions in some cell subpopulation frequencies

SARS-CoV-2 patients were subdivided based on the severity of the disease that was experienced by the patients. Patients who were admitted at the hospital (Haukeland University hospital or Haraldplass Diakonale Sykehus) were considered to have severe disease, while patients who did not require hospital admission were considered as mild/moderate. Duration and reason for admission were not reported, making it difficult to understand the grade of severity for the patients. Disease history and medication like immune suppressive was not reported.

Analyzing mild disease patients, severe disease patients, and healthy controls showed differences in subpopulation frequencies, but no significant differences are observed in any of the parent populations (Figure 19). All parent populations have FDR=0.05. As shown in figure 15A a large spread was seen in the CD4$^+$ central memory T cells among patients. Dividing them into moderate and severe, one did see a higher population frequency in the severe group, compared to CD8$^+$ central memory cells (figure 20). In figure 20A the differences within the patient group and control group are shown, a lower difference between the group is observed.

However, no significant difference is observed (FDR=0.177). $CD8^+$ effector T cells are slightly higher in the severe disease patient group, but differences within the group are high (figure 21).

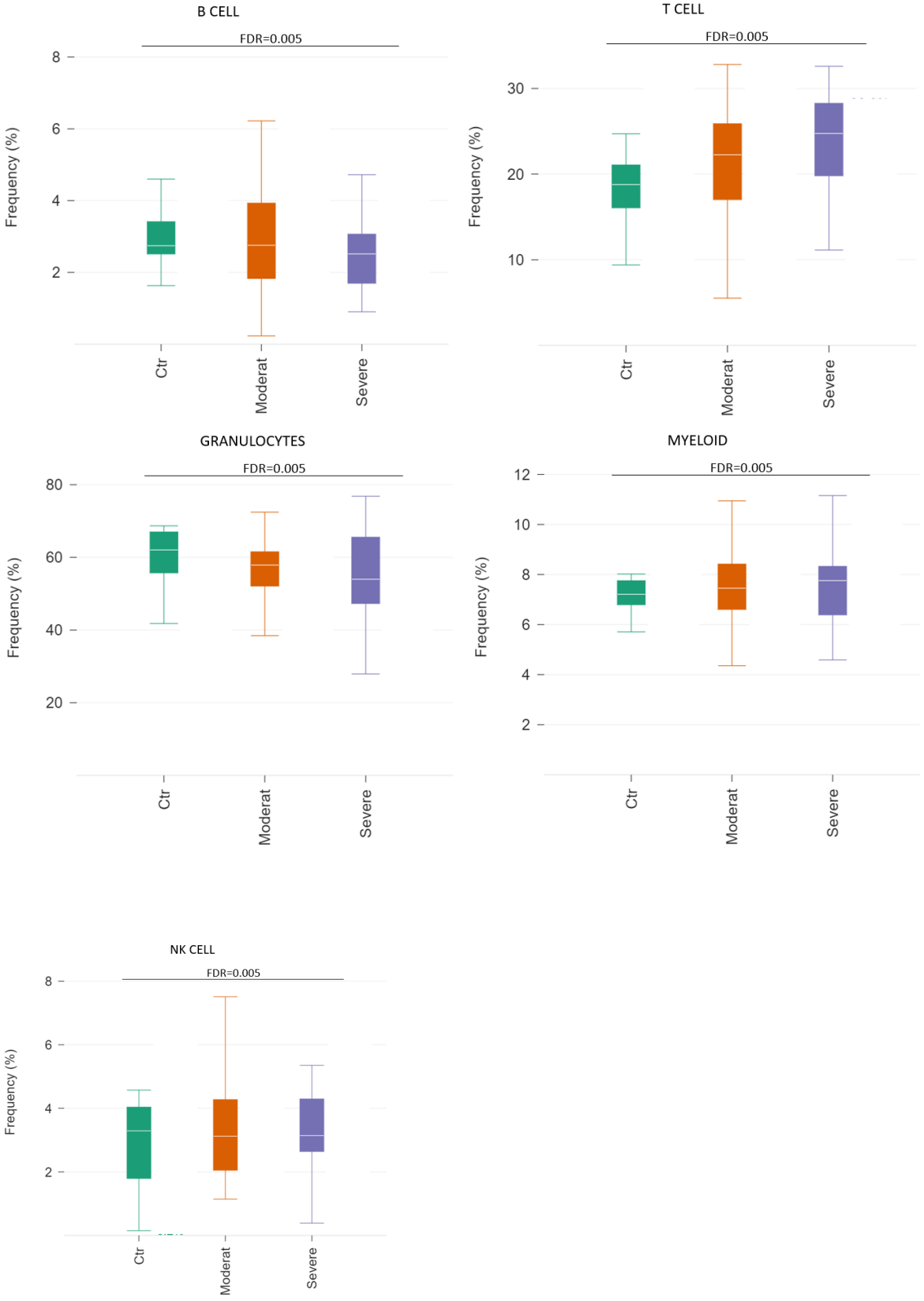

Figure 19 Overview of compartment populations in severe (n=14) and moderate (n=35) disease patients and healthy controls (n=10, ctr). *Comparisons were made among healthy controls/controls (n=10) and SARS-CoV-2 infected patients (n=49). Single-cell data was clustered together with FlowSOME R package with Ek'Balam algorithm labeling. Median for each cell population is stated and statistical significance is considered with FDR/adjusted for 0.05 ≥ p.*

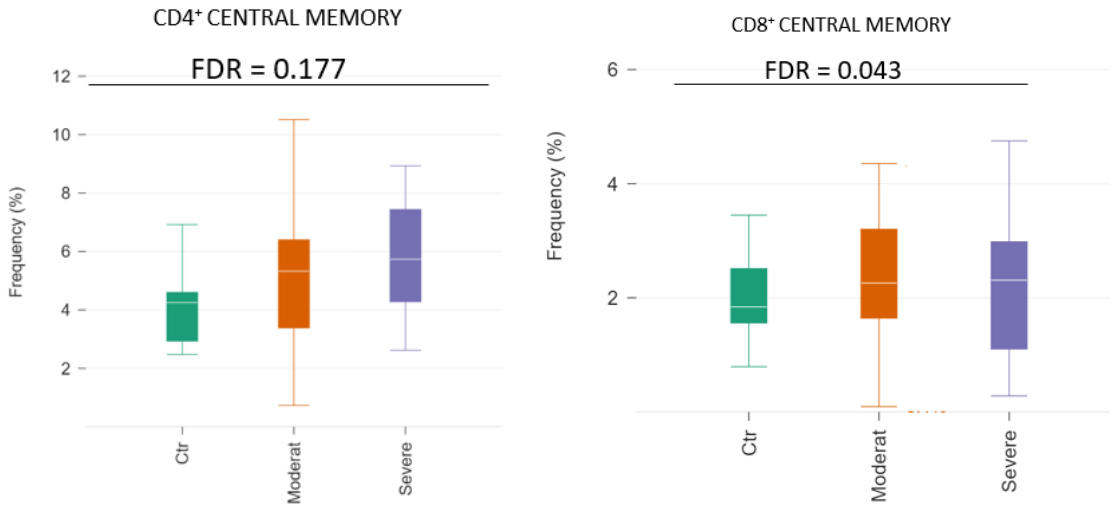

Figure 20 Central memory compartments in in healthy controls (n=10), moderate (n= 35) and severe patients (n=14). *A) CD4 + Central memory cell frequencies in healthy controls (n=10), moderate (n= 35) and severe patients (n=14). FDR=0.177. B) CD8+ central memory frequencies in healthy controls (n=10), moderate (n= 35) and severe patients (n=14). Single-cell data was clustered together with FlowSOME R package with Ek'Balam algorithm labeling. Median for each cell population is stated and statistical significance is considered with FDR/adjusted for 0.05 ≥ p.*

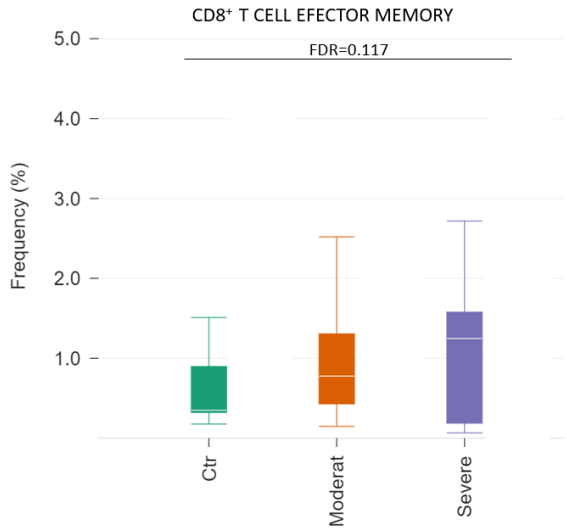

Figure 21 $CD8^+$ effector memory T cells in healthy controls (n=10), moderate (n=35) and severe (n=14) disease patients. FDR = 0.177. *Single-cell data was clustered together with FlowSOME R package with Ek'Balam algorithm labeling. Median for each cell population is stated and statistical significance is considered with FDR/adjusted for 0.05 ≥ p.*

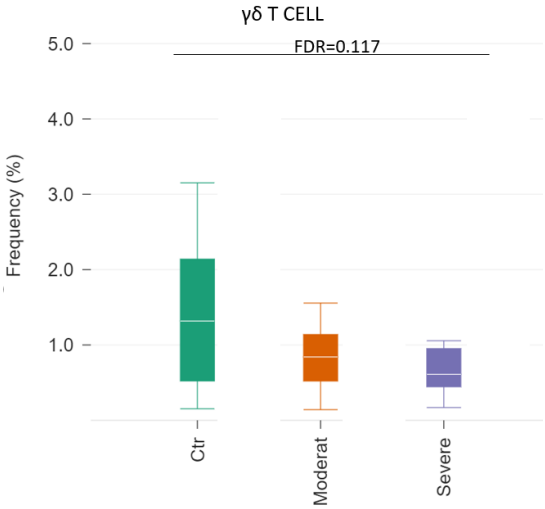

Figure 22 γδ T cell frequencies in healthy controls (n=10), moderate (n=35) and severe (n=14) disease patients. FDR=0.177. *Single-cell data was clustered together with FlowSOME R package with Ek'Balam algorithm labeling. Median for each cell population is stated and statistical significance is considered with FDR/adjusted for 0.05 ≥ p.*

Slight decrease in the significance was seen when γδ T cell frequencies (figure 22) were divided further. In the mild group, one sample that had initially low total cell count, shows remarkably elevated frequencies (>0.45).

3.2.1 Differences in monocyte subpopulations in moderate and severe patients

Investigating the change of non- and classical monocytes, we observed a decreasing pattern in frequency in the moderate group for classical monocytes (figure 23a). Four patients had higher frequency (>0.4%). Non-classical monocytes do not show large spread in the data compared to classical monocyte frequencies, and frequencies don't differ in the three groups.

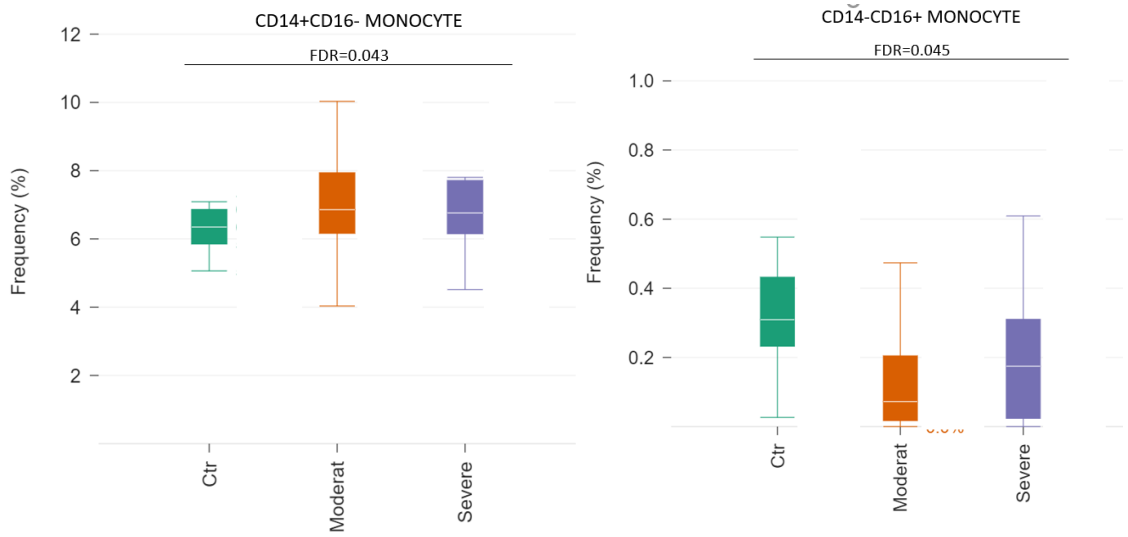

Figure 23 Monocytes compartments frequencies in healthy controls (n=10), moderate (n=35) and severe (n=14) disease patients. *A) CD14-CD16+ classical monocytes. FDR=0.043 B) CD14+CD16- non-classical monocytes. FDR=0.045. Single-cell data was clustered together with FlowSOME R package with Ek'Balam algorithm labeling. Median for each cell population is stated and statistical significance is considered with FDR/adjusted for 0.05 ≥ p.*

3.2.2 Wide variation among B cell phenotypes within convalescence COVID-19 patients and healthy controls

Normalized B cell frequencies in moderate and severe COVID-19 patients were found 6 months post infections. No differences in B cells in the control group and the patient group as a whole were detected (figure 24A). When characterizing B memory cell subsets depending on IgD expression, no significant differences were observed. However, compared to non-switched memory cells, bigger heterogeneity within the group was found in the switched memory B cell frequencies, suggesting different recovery (Figure 24B and 24C). Expansion of switched memory B cells in healthy control was also highly variable. Variation within the healthy controls might be a result of minimal exclusion criteria used for selection (figure 25).

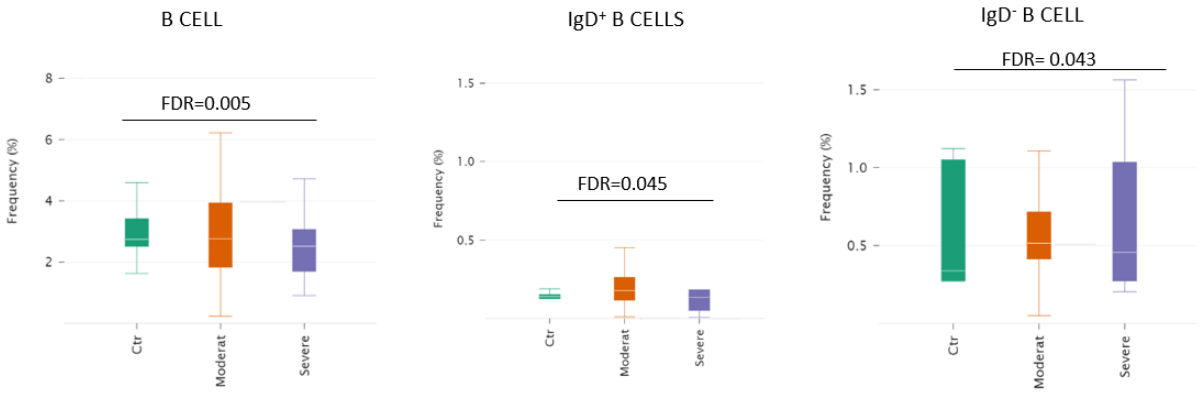

Figure 24 B cell compartments. A) Total B cell. FDR=0.005 *B) IgD$^+$ Non-Switched memory B cells frequencies in control, moderate and severe group. FDR=0.045 C) IgD$^-$ Switched memory B cell frequency in healthy controls, moderate and severe patient group. FDR=0.043 Single-cell data was clustered together with FlowSOME R package with Ek'Balam algorithm labeling. Median for each cell population is stated and statistical significance is considered with FDR/adjusted for 0.05 ≥ p.*

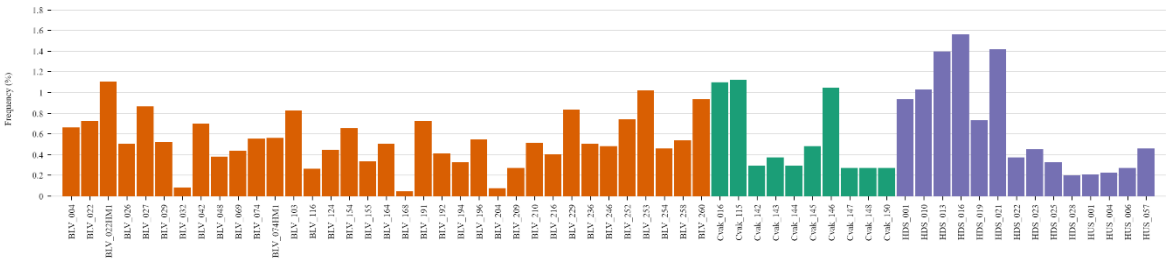

Figure 25 Frequencies of switched memory B cells within the individuals.

3.3 Age impact on our study samples

Due to highly variance data we choose to look at the impact of age immunological mechanisms so we could see if the variance/heterogeneity is SARS-Cov-2 dependent. Participants have been divided into three age groups as shown in table 1.

The same trend as seen for disease grade was observed, with no significant differences in parent cell populations rather in cell subsets. 6 months post-infection age-dependent variations in immunological aspects showed bigger difference (figure 26). Especially in naïve CD8$^+$ T cells and naïve B cells, significant lower frequencies in elderly (>65) patients as shown in figures 27 and 28.

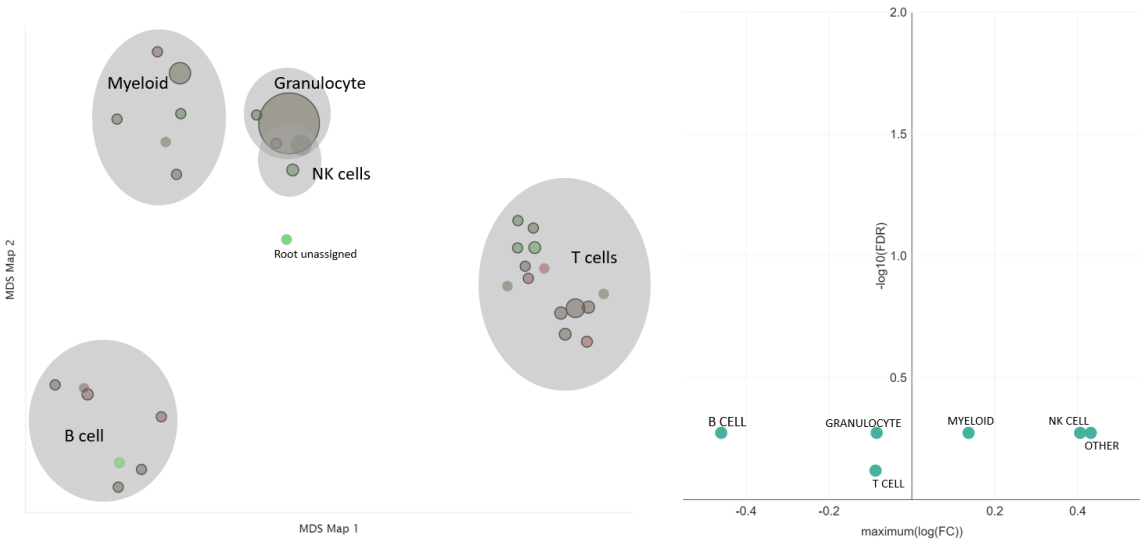

Figure 26 Overview of immune populations dependent on age *a) Differential abundance effect of age group cell subsets overview in a multidimensional scaling map (MDS) found by Astrolabe Diagnostics using labeling Ek'Balam algorithm (Amir et. al., 2019) and clustered together with FlowSOM R package (Van Gaseen et. al 2015). Frequency across all assigned subsets in a volcano plot based on age. False discovery rate (FDR), Fold change (FC).*

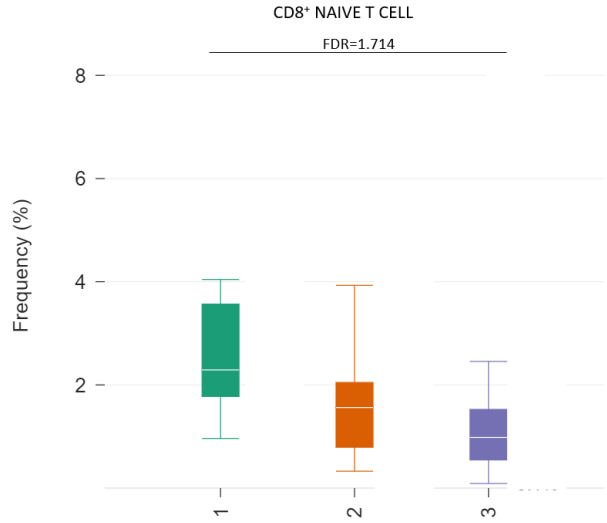

Figure 27 $CD8^+$ Naïve T cells differences between age group <40 (1), 40-60 (2) and >65 (3). FDR=1.714. *Single-cell data was clustered together with FlowSOME R package with Ek'Balam algorithm labeling. Median for each cell population is stated and statistical significance is considered with FDR/adjusted for 0.05 ≥ p.*

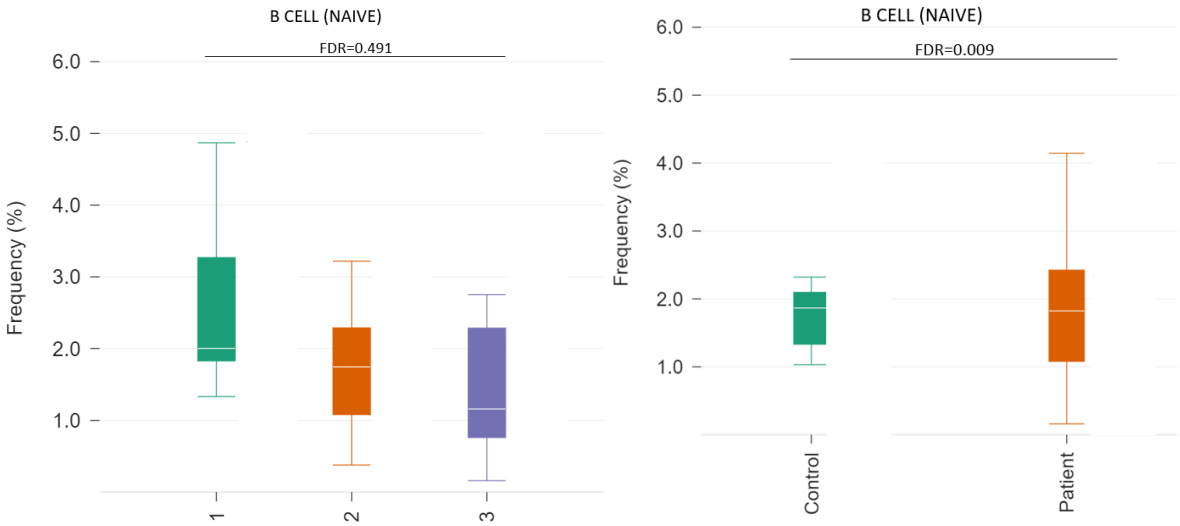

Figure 28 B naïve cell compartments in A) age group <40 (1), 40-60 (2) and >65 (3). FDR=0.491 B) healthy controls and SARS-CoV-2 patients. FDR=0.009. *Single-cell data was clustered together with FlowSOME R package with Ek'Balam algorithm labeling. Median for each cell population is stated and statistical significance is considered with FDR/adjusted for* $0.05 \geq p$.

3.2 Specific aim 2

3.2.1 Method development: Determining the cell density

Initial analysis for determination of the cell density was performed. HEK293, HEK293t and CACO-2 cells were seeded in 96 well plate for 24 hours with $2{,}5x10^3$, $5x10^3$, $1x10^4$, $2x10^4$, $4x10^4$ and $8x10^4$ for determining the optimal cell number for further analysis. Finding the right concentration is crucial for adequate confluency of the cells in the wells. As shown in figure 29, 2 x 10^4 and 4 x 10^4 cells per well gave good confluency and cell density after 24h, and therefore 3 $x10^4$ cells per well were chosen for both cell lines.

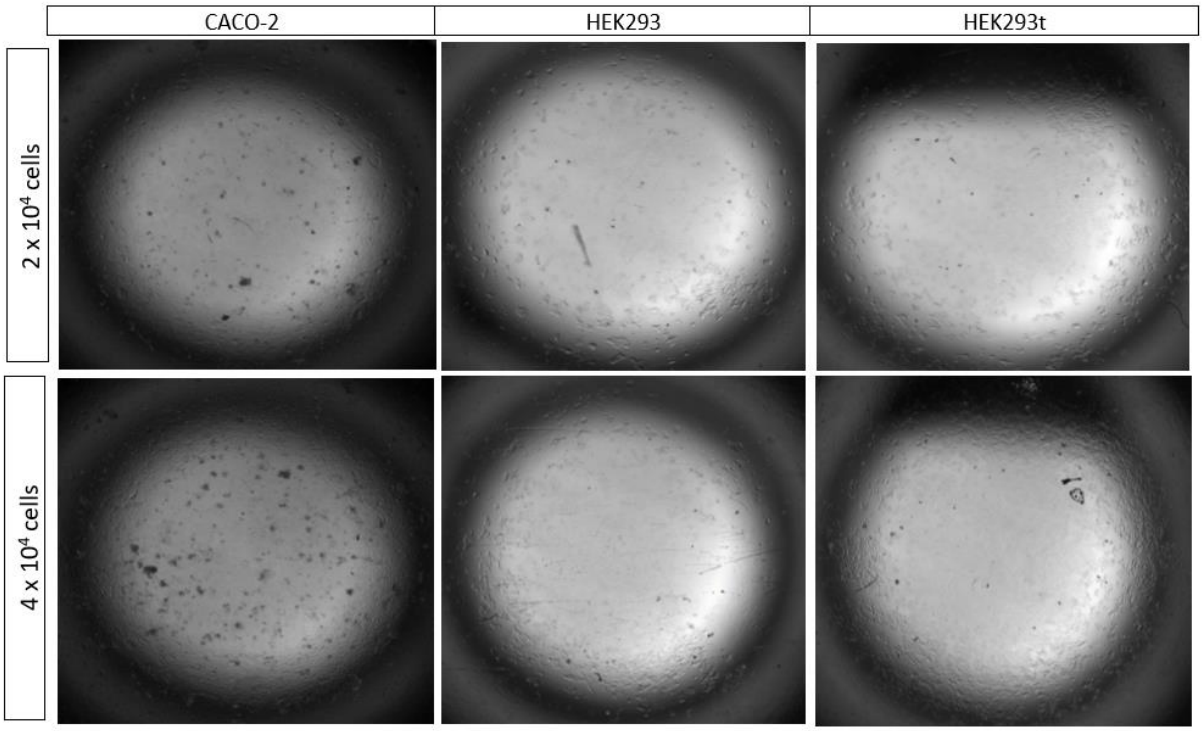

Figure 29 CACO-2, HEK293, and HEK293t cells seeded in 96 well plate. *2 x 10^4 and 4 x 10^4 cells were seeded per well in 96 well plate for 24h.*

3.1.2 Cell proliferation

CACO-2, HEK293, HEK293t cells were seeded and cultured with EA, RA, D7G, and PD in a 96 well plate with 3 x 10^4 cells per well for 24h. MTT assay was used for determination of proliferation and cell viability. On all three cell lines EA, RA, D7G, and PD were tested with different concentrations. EA and RA were tested with concentration at 10mM, 1 mM, 100 µM, 10µM, 1µM, 100nM and 10nM. For EA, an extra concentration at 1nM was additionally tested. For D7G concentrations at 1 mM, 100 µM, 10µM, 1µM, 100nM, 10nM, 1nM and 0,1nM was tested, while PD was tested with the same concentrations except from 1nM and 0,1 nM.

The higher the absorbance measured, the more metabolic active cells remain in the culture. For the HEK293 cell line (figure 30) the only remarkable change in the proliferation is for EA at high concentrations. EA shows a decreasing tendency in proliferation starting from 1µM, suggesting a dose-dependent response. For HEK293 cell lines variation between the triplicates shown through the ±standard deviation. Especially for EA, the standard deviation is remarkably higher for all concentrations, suggesting methodological errors.

For CACO-2 cells (figure 31) the same tendency is observed for EA. However, cell proliferation starts getting noticeably affected from 10 µM and higher concentrations. For the other tested substances, the proliferation remains unaffected.

In the HEK293t cell line (figure 32) the cell proliferation shows effect by PD and D7G from 0.01mM and higher concentrations. For EA effecting concentration starts from 0.1mM and shows a stronger response for higher concentrations. For RA it was expected the same effects as the other cell lines or that the proliferation decreases with higher concentrations. However, the opposite was observed arising questions about the possibility of methodological errors disturb the result considerably. Due to time constraints re-acquisition of the experiment could not find place.

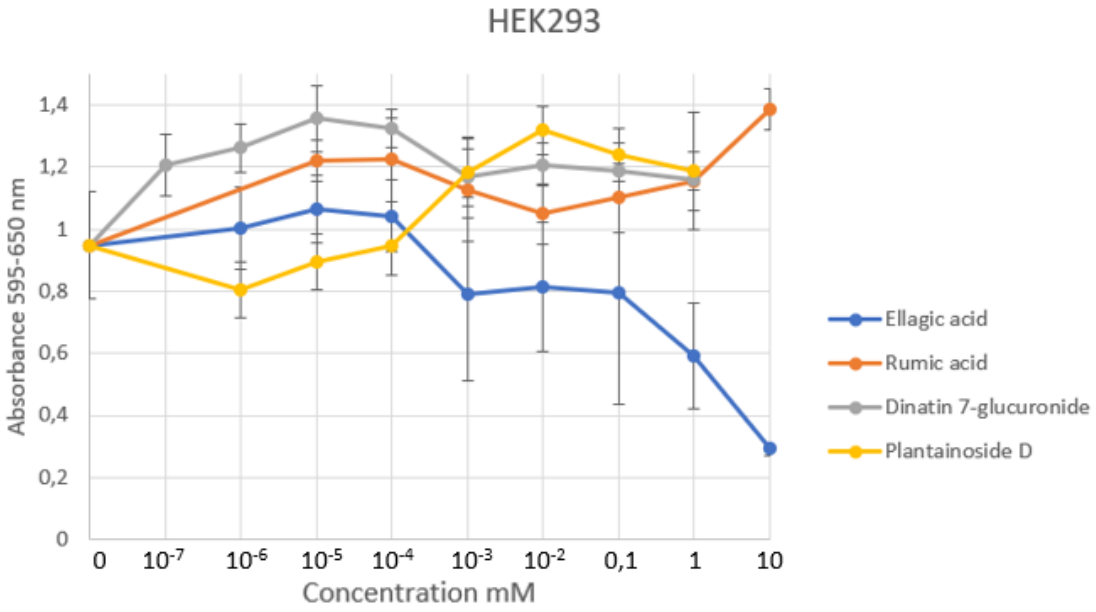

Figure 30 Proliferation of HEK293 cells in response to Ellagic acid, Rumic acid, Dinatin 7-glucuronide, and Plantainoside D using MTT assay. *Figure shows three replicates.*

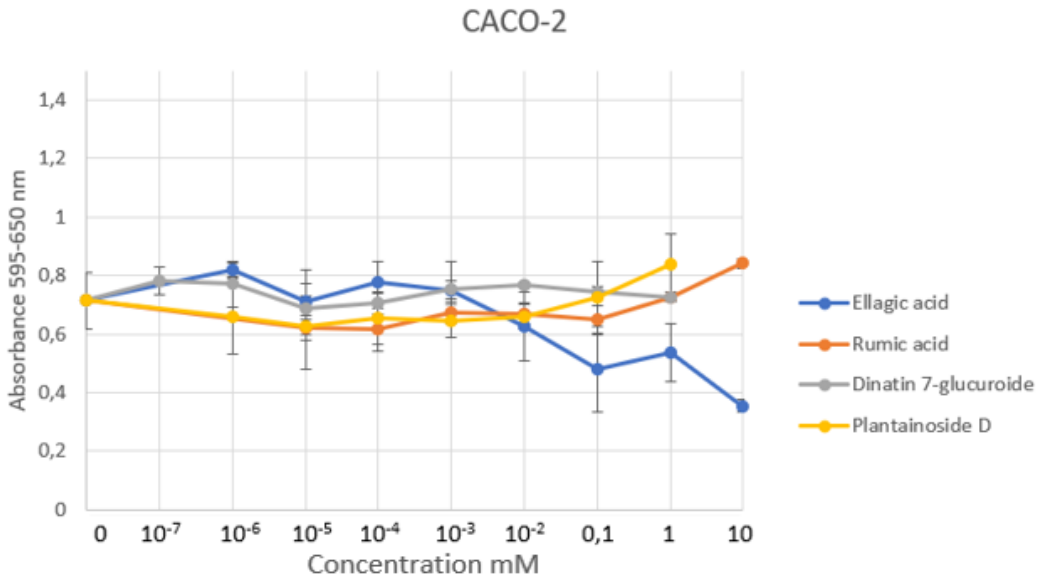

Figure 31 Proliferation of CACO-2 cells in response to Ellagic acid, Rumic acid, Dinatin 7-glucuronide, and Plantainoside D using MTT assay. *Figure shows three replicates.*

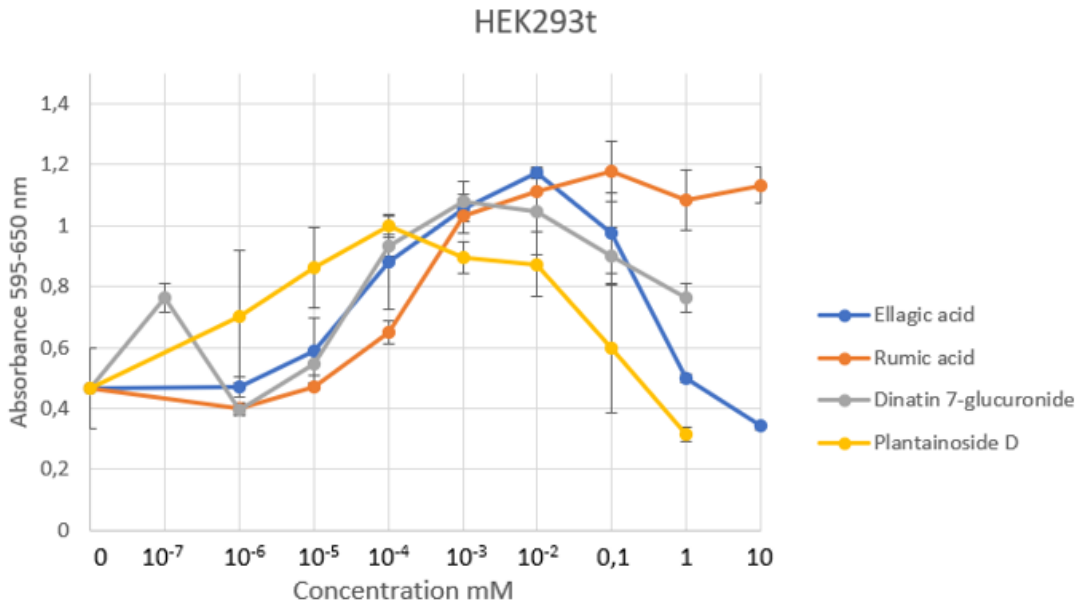

Figure 32 proliferation of HEK293t cells in response to Ellagic acid, Rumic acid, Dinatin 7-glucuronide, and Plantainoside D using MTT assay. *Figure show three replicates*

When seeding the cell cultures, 6 wells in the 96-well plate were not exposed for the substances, and these were used as controls. As shown in table 5 all three cell lines had variation in the control well, but the biggest variation was observed in HEK293t cell line. Ideally, the control values are supposed to have similar values. All graphs start with the mean value of all 6 controls.

Table 5 Absorbance at 590nm, mean value and standard deviation for control values in HEK293, CACO-2, and HEK293t cell lines

	HEK293	CACO-2	HEK293t
Controls	1,106	0,766	0,418
	1,093	0,708	0,384
	1,104	0,657	0,392
	0,852	0,799	0,732
	0,772	0,807	0,423
	0,752	0,552	0,450
Mean	0,095	0,715	0,467
Standard deviation	0,175	0,098	0,132

4. Discussion

4.1 Specific aim 1

Exploiting mass cytometry, this study identified multiple blood immune cell subsets in SARS-CoV-2 infected patients 6 months post-infection. Mainly, populations that showed alterations in the study group have been focused on. Previously few available studies have investigated mass cytometric analysis with only extracellular markers on SARS-CoV-2 infected patients. In addition, very little is known about unique aspects in SARS-CoV-2 pathogenesis and much of the published data suffer from internal and external thorough validation.

Heterogenicity among individuals found in this study is highly believed to be SARS-CoV-2 specific. Looking at, age-related differences in the immune system data shows homogeneity in accordance with science and already knowledge about the immune system. Other factors, such as disease history, weight, and medication, can affect the immune system and recovery after SARS-CoV-2 infection.

Comparing the control group and the patient group, no significant differences could be seen in any of the parent populations, but in some subpopulations, differences were found. $CD4^+$ central memory and gamma delta T cell subset altered non significantly. For $CD4^+$ central memory cells, we saw a large spread in the data that came from three samples in the patient group that showed relatively low frequencies of $CD4^+$ central memory cells. In addition, one of these samples had an extremely low total cell number (total cell number: 19 710 cells).

Rodriguez *et. al. 2020* (64) have reported that $CD127^+$ memory $CD4^+$ cells have a decreasing pattern 26 days post-infection. Findings from our study show the opposite with slight increased $CD4^+$ central memory cells which are in accordance with Dan *et. al 2021 (65)*. These findings suggest that $CD4^+$ central memory cells increase after the acute and early phases. Studies have shown that $CD4^+$ T cells are affected by lymphopenia, and severe cases have lower levels of total lymphocytes, such as $CD4^+$ T cells, $CD8^+$ T cells, and B cells (Wang et al 2020, (66)). If any of our patients did suffer from lymphopenia, our data suggest that the lymphopenia does not remain post 6 months. Previously Silvin *et. al*. 2020 (67) have found that the overall monocyte population was non-significant between healthy controls and patients when the infection occurs. However, looking into subsets significant differences were observed. In accordance with their findings, we disclosed that $CD14^-CD16^+$ non-classical monocytes had a slightly lower frequency in the patient group than control group, although it was not significant. $CD16^+$ monocyte decreases are SARS-CoV-2 specific since $CD16^+$ monocytes have previously been reported to be dominant in bacterial diseases and viral infections. (68)

In classical monocytes, there were no differences between the patient group and the control group. Classical monocytes have previously been described to be lower in the acute phase of COVID-19 but showing elevating concentrations in the recovery phase (Rodriguez et.al 2020, (64)). Increased classical monocytes indicate that the monocytes go back to their initial concentrations 6 months post infections. Although no alteration between the patient group and healthy control was observed in our data, a variation between individuals was observed. These variations can be caused by genetic variation between individuals and low cell count in some of the samples. Variation in the human immune system due to genetic variations generally and in COVID-19 needs to be investigated (69).

In other viral infection, γδ T cells tend to increase in acute viral infections, but in COVID-19 patients this cell subtype has shown decreased frequencies, suggesting that γδ T cells are affected in different ways depending on the virus (40). Rodriguez et al 2020 showed increase frequencies of different subtypes of γδ T cells, suggesting recovery of γδ T cells after 1 month (64). Normally γδ T cells are approximately around 5% of the peripheral blood (70), in our data shows around ~1% median value of γδ T cells in peripheral blood, which is lower, and thereby suggest not fully recovery of the immune system. Looking at γδ T cell frequencies (figure 22) in moderate and severe cases recovery among severe patients seems to be slower. In the mild group, one sample that had initially low total cell count shows remarkably elevated frequencies (>0.45).

Similarly, to Rodrigues et al 2020, we experienced high variating data in both conventional and plasmacytoid dendritic cells. In our data, we experienced high variation between our controls and patient group, which reflects issues with low total cell numbers in samples caused by debris.

B cells in convalescent patients showed heterogenicity and lack of similar trends within the individuals, making it difficult to conclude whether the B cell subsets are restored 6 months post-infection. Rodriguez et. al. 2020 and Shuwa et. al 2021 reported a decreasing trend in unswitched memory B cells in contrast with increasing trend in switched B cells, which is in line with findings in this study with equality frequencies in patients and healthy controls (64, 71). We experienced wide heterogenicity within individuals for switched B cell frequencies, suggesting recovery is affected by other factors, such as genetic variation, severity, comorbidities etc., then only time. Wide heterogeneity among individuals in the same group also indicates that COVID-19 patients should be subdivided based on the lymphocyte phenotypes and then compared in order to find clear similarities.

Next, we investigated age differences among the study group to strengthen our theory about SARS-Cov-2 induced heterogeneity within our data. $CD8^+$ naïve T cells and naïve B cells were significantly lower in higher age groups. It is previously known that naïve cells decrease proportionally with increased memory cells and age (1). Other research groups that investigate immune cells in peripheral blood of COVID-19 patients, such as Newell et. al. 2021 also experienced heterogeneity in SARS-CoV-2 convalescence patients (72).

Taken together, we expected SARS-CoV-2 infected patients to have recovered from COVID-19 and thereby have similar immune system composition as non-infected SARS-CoV-2 individuals. However, we report differences in adaptive immune cell subsets, such as $CD4^+$ central memory T cell and switched memory B cells 6 months post-infection. Lack of homogeneity in different papers challenges making any concluding remarks.

4.1.1 Mass cytometry versus flow cytometry

Mass cytometer is an explorative method that can detect more than 40 targets with a single cell panel and can analyze a broad range of immunological aspects. Using more than 17 markers in flow cytometer analysis is relative seldom, due to issues with spectral overlap. Running flow cytometry can risk of giving autofluorescence and spectral overlap. In comparison with the flow cytometer, mass cytometer does not have these factors affecting the data, and thereby has a lower range of background noise.

The range of intensities differs in both methods, whereas the metal isotopes in mass cytometry has almost the same signal intensity, while in flow cytometry the different fluorophores have a broader range of intensities. Complexity of the panel is affected by the signal intensity, but detection of low expressed cell populations/molecules. Resulting that mass cytometry is the preferred method in explorative experiments, while flow cytometry is preferred to investigate further specific targets/molecules. However, events in massy cytometry get lost before it reaches the detector, making it a less sensitive method compared to flow cytometry.

Using mass cytometry limits some information that can be provided by using flow cytometry. Firstly, in mass cytometry analysis, the information about the granularity size of the cells cannot be provided since measurement of forward scatter and side scatter is not possible. Secondly, fluorophores used in flow cytometry have higher sensitivity than the lanthanide metals that are used in mass cytometry. Thirdly, mass cytometric measurements limit 500 cells per second resulting in a more time-consuming technique. Lastly, in mass cytometry sorting of the cells is not possible, since all biological material is removed before the analysis (54). Furthermore,

mass cytometric analysis is relatively expensive resulting in low availability of mass cytometers.

4.1.2 Methodological considerations

Large-scale data experience challenges regarding quality control, batch effect, and laboratory variability. Impact on this on data in this study, was highly replicable in each sample's total cell count. In addition to the loss of cell events due to poor fixation and lysis of the cells, removing debris can cause loss of cell events, along with doublets and bead normalization. In some samples, extremely low total cell count (> 20 000) was identified, which can affect some populations frequencies in the analysis.

4.1.2.1 Contamination/background noise

Contamination/background noise: In biological materials metal isotopes from the rear-earth metals should not occur, resulting in no endogenous cellular background. Sources of contamination that can interfere with the analysis can be Barium (137-138 Ba), Iodide (127 I), and Lead (208Pb). Sources of Barium can be contaminated bovine serum albumin (BSA) and some lab and sample preparation equipment like rubber. Core Facility for Flow cytometry has discovered that latex-free gloves can be a source for Barium. Iodide contamination usually comes from remnants of salts from reagents preparing samples, like PBS. samples contaminated with lead have usually been processed with reagents prepared and stored in glass ware. To reduce the risk for contamination, choice of reagents, lab equipment, and washing procedures were chosen with high precautions.

4.1.2.2 Antibody titration:

Minimizing the spillover, antibodies were titrated to distinguish the optimal staining concentrations benefiting experimental conditions. The premade antibody panel used in this project had already titrated most of the antibodies. Adjustments for IgA (Chapter 2.1.2.4) was performed, and antibodies that were sensitive to fixation were removed. However, IgA was adjusted and titrated it was seen to be too high concentration of IgA in the analysis. This is most likely caused by errors while pipetting when titrating or making the antibody cocktail. Although, high concentrations of IgA were observed, it gave low impact on the main analysis due to the labeling hierarchy/gating.

4.1.2.3 Freezing and thawing of cells

Massive sample handling with limited staff during the national lockdown in 2020 due to the pandemic resulted in variable quality of samples of the cryopreserved peripheral blood mononuclear cells (PBMCs). Due to the large variability of sample quality of the cryopreserved

PBMCs, samples acquired when participants had COVID-19 (timepoint zero) could not be analyzed and had to be excluded from this study. Not having data from timepoint zero has caused difficulties to conclude whether recovery among the patients happens and to understand the heterogenicity.

Using the fixed whole blood preservation leads to accurate replication of all cell composition in the peripheral blood. Cryopreserving PBMC using density separation results in altered basophils and eosinophils and excluding neutrophils that can not be frozen and thawed without massive cell death (73, 74). Whole blood preservation requires less blood volume which is beneficial in pediatric and critically ill patients. Therefore, the method of choice for sample gathering 6 months post-infection was changed to stable fixation of whole blood.

Thawing the fixed whole blood cells was done rapidly at 37^{o}C water bath, to regain cell viability and recovery by reducing the chances for recrystallizing and osmotic stress (75). While removing red blood cells from the fixated whole blood it was experienced problems in achieving fully white pellet in some samples. These samples had red pellet even after undergoing the lysis process twice (CP-HUS 57, PAS-HDS 22, PAS-BLV 252, PAS-BLV 0253, PAS-BLV 0032, PAS-HDS 01, PAS-HDS 21, PAS-BLV 069, PAS BLV 0152), arising question about poor mixing of stabilizer in the fixation process or plasma factors, such as polymerized fibrin affecting the lysis process. However, COVID-19 disease-associated coagulopathy was excluded as a possibility since the same occurrence was found in the healthy controls.

Removing the remaining red blood cells with sorting was tried in the methodology development but resulted in low numbers of total cell count, and therefore excluded from the main experiment. In the sample preparation, it was experienced struggles to achieve a completely white pellet, even after washing several times. Having red blood cells in the sample results in debris that disturb the analysis with giving a higher fraction of poor/bad events will occur.

4.2 Specific aim 2

Effects of ellagic acid, rumic acid, dinatin 7-glucuronide, and plantainoside D on cell proliferation were investigated by MTT assay on HEK293, HEK293t, and CACO-2 cells in 24 hours incubation period.

In all three cell lines, our data (figure 30, 31, and 32) suggest EA had a dose-dependent response effect on the metabolic active cells. In the CACO-2 cells, the other tested substances had a homogenous absorbance value, suggesting low impact of tested drugs on the cells. An overall overview on the standard deviation (supplementary) for all substances tested in CACO-2 cell lines, shows that triplicates are not varying a lot. The opposite is discovered in HEK293 and HEK293t cell lines, where a bigger difference between the triplets, along with the control values was seen, resulting in difficulties to make any concluding remarks whether EA, RA, D7G and PD have an influence on the cells.

Although EA has previously been reported (76) to be soluble in DMSO, it was experienced issues with solubilization in this study. Studies, such as Byrne et. al, 2008 have shown that EA has poor aqueous solubility characteristics, suggesting DMSO would be a good choice of solvent (77). However, the data from this study replicates segmentation of the compound, suggesting poor solubilization of ellagic acid in DMSO. Reasons behind segmentations occurring are still unknown, but ideally, ellagic acid with same concentrations should have been tested again with DMSO or another solvent, but due to lack of time this could not be conducted.

Cell-based assay, such as MTT assay, have numerous flaws and limitations. In MTT assay formation of water insoluble purple formazan crystals from tetrazolium salt, occur in live cells with the help of mitochondrial succinate dehydrogenase enzyme. However, it has previously been reported that some phytochemicals can affect mitochondrial succinate dehydrogenase with can give inconsistent results (78, 79). Phytochemicals used in this study is newly developed, and therefore limited studies have been published regarding their effect on MTT assays. However, previous studies (Li et al., 2018, Kumar et al., 2016) on determination of cell proliferation after EA exposure have shown that EA have a dose- and time-dependent response (80, 81). Other compounds tested in this study are relevantly new compounds that have limited studies available. No previously studies were found where MTT assay was used for detecting cytotoxicity on cells using these compounds, arising question whether a potential interaction might be true.

In the MTT assay exponentially growing cells metabolic activity are measured, but exposure of substances on the cells gives a possibility for delayed growth and metabolic activity. This statement arises questions about whether the substances tested in this study perhaps have a time-dependent effect. Therefore, other timepoints, such as 48h, 72h and 96 hours, should have been measured. In this project MTT assay was supposed to be confirmed with other apoptosis assays, such as Annexin staining assay. In that way apoptotic cells could be measured and subdivided between early and late apoptotic cells. Another advantage with Annexin assay, is that this method does not rely on cell density in the same manner as MTT assay for detection of apoptotic cells. This would eliminate the problem with heterogeneous cell number observed in this study (Table 5).

4.2.1 Methodological consideration

Proliferation of cells can give a good indication of tolerance of chemical substances. Using MTT assay can be used as first step in determining the drug effect of ellagic acid, rumic acid, dinatin-7 glucuronide and plantainoside D on different cell types. In this study it has not been showed clear results, which might be the result of using MTT assay. MTT assay has large variation, resulting in that MTT assay do not have the ability to detect small changes in the cell viability/proliferation (82). Chemical compounds can have a different effect, such as cytotoxicity, depending on the cell density, since cell density can correspond with oxidative stress resistance. (83)

The number of cells and cell density in each well are critical for the MTT assay and for detecting drug toxicity. Accordingly to the manufacture (84), optimal seeding density is achieved with around 1 x 10^4 cells per well, however in this study the number were chosen to be 3 x 10^4. Using a higher number of cells, as recommended from the manufacture, was based on the evaluation for reaching optimal confluency after 24 hours.

Counting cells with a hemocytometer is a subjective approach, resulting in higher variation in counting technique. Although using a hemocytometer is a time-consuming technique compared to other methods available on the market, it is a low-cost technique. Adherent cells tend aggregate within few minutes, leading to cells not being equally distributed in the suspension, which can lead to influence on the suspension homogeneity. This leads to challenges during manual counting and while breaking up the clusters without effecting the cell viability. To overcome these challenges suspension was gently mixed with a pipette for increasing the homogeneity.

5. Limitations of the study

5.1 Specific aim 1

While carrying out this research, different factors limited the study. The study population size was a compromise between the ability to identify differences and feasibility, such as expensive reagents and laboratory approaches. More SARS-CoV-2 infected individuals that had been discharged from the hospital should have been included in the cohort. Having few individuals can affect the statistical significance of individual parameters negatively.

Healthy individuals were used as the control group in this study. The number of healthy controls were limited since the ethical approval of the project was connected to a bigger project which is limited to healthcare workers. Although, relevant information about the healthy control, such as age and sex were gathered, information about negative COVID-19 test were lacking, arising questions about slight chances that unknowingly these individuals have been exposed to SARS-CoV-2 and developed immune responses.

Limited information regarding some clinical parameters resulted in difficulties to subdivide the cohort groups further. In participants characteristics (table 1), comorbidities and BMI are considered as one parameter showing an unclear understanding how these to parameters effect the immune response separately. Details about comorbidities and how this parameter was defined by the samplers remains unknown. Other parameters such as medical history and fatigue are also limited in this study.

Collection of blood samples for the project were done over time and we wanted to analyze them together, the samples were therefore cryopreserved within an hour after collection. As mentioned before blood samples were fixed whole blood and ideally it will not affect the cell recovery and intracellular signaling. However, we experienced that some of the samples had a thick consistency after thawing, suggesting that the fixation solution was not mixed properly. Patient samples had a longer cryopreservation time than the healthy controls giving a higher inter-individual variation in terms of storage.

For the cytometric analysis, some limitations occurred. Firstly, we experienced low numbers of cells in some patients that effect on the analysis of some cell populations (e.g., classical monocytes). Secondly, wide heterogeneity among the group resulted in challenges determining clear differences dependent on disease severity. Finally, analyzing whole blood gives high frequencies of granulocytes and difficulties to separate them occurs when putting CD66b and

TCRγδ on the same metal tag. Therefore, looking at the γδT cell population some biased results might be expected.

In this study whole blood was studied, but primarily COVID-19 is a pulmonary disease, and a more accurate overview of the immune responses will be achieved with alveolar samples. However, in this study peripheral whole blood was analyzed.

5.2 Specific aim 2

For the MTT assay the biggest limitation was time restrictions. Due to the pandemic, lab work started later than expected, resulting in no time for acquisition of plate replicates, especially with Ellagic acid the analysis should have been redone. However, this is an ongoing study that will proceed and analyze in-depth potential natural compounds that can affect SARS-CoV-2.

6. Future perspectives

6.1 Specific aim 1

Infection with SARS-CoV-2 is a fast-mutating virus that has resulted in fatal complications such as severe acute respiratory syndrome and in worst cases death. Worldwide an enormous investigating is ongoing to understand the immune response in human against SARS-CoV-2. This is important for developing treatments and vaccines that has good effect in the existing and mutated version of SARS-CoV-2. The results presented in this thesis aim to increase the understanding of the immune responses against the virus and to find potential candidates for drug treatment against the virus. However, some questions about immunity development against the virus remains unclear and unanswered. In addition, therapeutic strategies need to be determined and explored.

Based the result of this project, further studies should include analyzing the longitudinal blood samples gathered up to 9 months and 12 months post SARS-CoV-2 infection of the participants. Knowing the immunological aspect after 9 and 12 months will give an impact on how the immunity will change and show a better understanding.

Another interesting angle of this project would have been to compare the immunological development in SARS-CoV-2 infected patients with individuals that has been infected with some of the mutated variants of the virus. To compare these groups will give an insight on the immunological differences and a better understanding on how the treatments can differ for the native virus and mutated virus. Include COVID-19 vaccinated individuals and compare the differences in the immunity with the group included in this study would also have been interesting.

Using peripheral blood in this study is due to availability and advantages regarding biomarker discovery. However, to fully understand COVID-19 pathophysiology it is important to investigate the active site of the disease, which in this case will be the lungs. Imaging mass cytometry analysis of lung biopsies will provide multiple markers visualization in tissue sections. Thus, interplay of cell subsets involved in COVID-19 can be discovered.

6.2 Specific aim 2

In this study the MTT assay approach to find a potential COVID-19 drug treatment were limited and did not give a clear understanding if the compound tested had a cytotoxic on the cell cultures. However, what have been done with the testing of potential drugs against COVID-19 in this study is a start of a bigger study that includes testing at least 19 naturally extracted

substances received from Torgils Fossens group Natural Products Chemistry and Pharmacognosy.

Although, Ellagic acid was tested in this study, further studies must be done considering this compound. In this study issues regarding the solvent occurred and gave a biased result since the active compound most likely segregated. Changing the solvent and analyzing with MTT assay again will show a better understanding if the compound has a cytotoxic effect on human cells. Importantly, this study only included testing on 24h exposure, longer exposure need to be analyzed.

In addition, it will be interesting to explore whether the compounds show different effects using other assays, such as Annexin Assay. After finding the potential cytotoxic effect for Ellagic acid, Rumic acid, dinatin 7-glucorunide and plantainoside D, these compounds need to be tested against the SARS-CoV-2 virus. This can for example be done with qPCR.

Cells used in this study originated from primary cell cultures. Cell lines subcultured from parental tissue can have generated genetic and phenotypic alterations during the process leading to loss of important characteristics from the original tissue. Importantly, cells that differs from original tissue can provide false negative or false positive findings due to low resemblance of the in-vitro environment. For future projects this should be considered, and effects from the compound should be double-checked with primary cells.

Conclusion

In COVID-19 recovered patients it was found increased trend of $CD4^+$ central T cells and switched B cells. Along with data suggesting not fully recovery of γδ T cells and $CD14^-CD16^+$ monocytes.

Taken together, differences in adaptive immune cell subsets were found, in $CD4^+$ central memory T cell and switched memory B cells differences between healthy controls and SARS-CoV-2 infected patients were found 6 months post-infection. However, we experienced a heterogenicity among the study group that we believe is SARS-CoV-2 specific.

For the MTT assay we could not conclude whether the Ellagic acid, rumic acid, dinatin 7-glucuronide, and Plantainoside D had any effect on HEK293, HEK293t and CACO-2 cells. Further studies must be done to get better understanding.

References

1. Abbas AK, Litchman, Andrew H., Pillai, Shiv., . Basic immunology: functions and disorders of the immune system 6th ed2020.
2. Su D-L, Lu Z-M, Shen M-N, Li X, Sun L-Y. Roles of Pro- and Anti-Inflammatory Cytokines in the Pathogenesis of SLE. Journal of Biomedicine and Biotechnology. 2012;2012:347141.
3. Gil-Etayo FJ, Suàrez-Fernández P, Cabrera-Marante O, Arroyo D, Garcinuño S, Naranjo L, et al. T-Helper Cell Subset Response Is a Determining Factor in COVID-19 Progression. Front Cell Infect Microbiol. 2021;11:624483-.
4. Kahn JS, McIntosh K. History and Recent Advances in Coronavirus Discovery. The Pediatric Infectious Disease Journal. 2005;24(11):S223-S7.
5. WHO Who. CORONAVIRUS [internet]. Who.int: World health organization 2020 [cited 2020 22. november]. Available from: https://www.who.int/health-topics/coronavirus#tab=tab_1.
6. Organization WH. Middle East Respiratory syndrome Coronavirus (MERS-CoV) Switzerland [cited 2020 05.10]. Available from: https://www.who.int/emergencies/mers-cov/en/.
7. Organization. WH. Severe acute respiratory syndrome Switzerland: World Health Organization 2020 [cited 2020 05.10]. Available from: https://www.who.int/ith/diseases/sars/en/.
8. McIntosh K. Coronavirus disease 2019 (COVID-19): Epidemiology, virology, and prevention USA: UpToDate; 2020 [updated Sept 29, 2020; cited 2020 05.10.2020]. Available from: https://www.uptodate.com/contents/coronavirus-disease-2019-covid-19-epidemiology-virology-and-prevention#H4014462337.
9. WHO Who. Zoonotic disease: emerging public health threats in the Region Switzerland [cited 2020 19. November]. Available from: http://www.emro.who.int/about-who/rc61/zoonotic-diseases.html.
10. Andersen KG, Rambaut A, Lipkin WI, Holmes EC, Garry RF. The proximal origin of SARS-CoV-2. Nature Medicine. 2020;26(4):450-2.
11. WHO Who. Transmission of SARS-CoV-2: implications for infection prevention precautions Internet World health organization 2020 [cited 2020 22. November].
12. Kumar A, Prasoon P, Kumari C, Pareek V, Faiq MA, Narayan RK, et al. SARS-CoV-2-specific virulence factors in COVID-19. Journal of Medical Virology. 2020;n/a(n/a).
13. Xia S, Lan Q, Su S, Wang X, Xu W, Liu Z, et al. The role of furin cleavage site in SARS-CoV-2 spike protein-mediated membrane fusion in the presence or absence of trypsin. Signal Transduction and Targeted Therapy. 2020;5(1):92.
14. Ian Fenna. SARS-CoV-2 (2019-nCoV) Proteins Crech Republic Biovendor 2020 [updated 23.03.2020; cited 2020 09.24]. Available from: https://www.biovendor.com/sars-cov-2-2019-ncov-proteins?utm_source=google&utm_medium=organic.
15. Goldman E. Exaggerated risk of transmission of COVID-19 by fomites. Lancet Infect Dis. 2020;20(8):892-3.
16. Mittal R, Ni R, Seo J-H. The flow physics of COVID-19. Journal of fluid Mechanics. 2020;894.
17. Bourouiba L. Turbulent Gas Clouds and Respiratory Pathogen Emissions: Potential Implications for Reducing Transmission of COVID-19. JAMA. 2020;323(18):1837-8.
18. Wang W, Xu Y, Gao R, Lu R, Han K, Wu G, et al. Detection of SARS-CoV-2 in Different Types of Clinical Specimens. Jama. 2020;323(18):1843-4.
19. Cao Z, Li T, Liang L, Wang H, Wei F, Meng S, et al. Clinical characteristics of Coronavirus Disease 2019 patients in Beijing, China. PLOS ONE. 2020;15(6):e0234764.
20. Folkehelseinstituttet (FHI). Sars (Severe Acute Respiratory Syndrome) - Veileder for helsepersonell Oslo2010 [updated 07.07.2019; cited 2020. 23.09]. Available from: https://www.fhi.no/nettpub/smittevernveilederen/sykdommer-a-a/sars-og-mers-alvorlige-coronavirusi/.
21. Bianca N. What the data say about asymptomatic COVID infections [Journal]. nature.com 2020 [updated 23. November 2020; cited 2020 23. november]. Available from: https://www.nature.com/articles/d41586-020-03141-3.

22. Johannesen T. Long Covid Internet Norsk helseinformatikk 2021 [Available from: https://nhi.no/for-helsepersonell/fra-vitenskapen/langvarig-covid-long-covid/.
23. Himmels JPW QS, Brurberg KG, Gravningen KM. Langvarige effekter av covid-19. Hurtigoversikt. Skøyen; 2021.
24. Trougakos IP, Stamatelopoulos K, Terpos E, Tsitsilonis OE, Aivalioti E, Paraskevis D, et al. Insights to SARS-CoV-2 life cycle, pathophysiology, and rationalized treatments that target COVID-19 clinical complications. Journal of Biomedical Science. 2021;28(1):9.
25. Vellas C, Delobel P, De Souto Barreto P, Izopet J. COVID-19, Virology and Geroscience: A Perspective. The journal of nutrition, health & aging. 2020;24(7):685-91.
26. Folkehelseinstituttet (FHI). MERS - Middle East Respiratory Syndrome Coronavirus (MERS-CoV) Oslo2013 [updated 26.11.2018; cited 2020 23.09]. Available from: https://www.fhi.no/sv/smittsomme-sykdommer/corona/mers/om-mers/.
27. V'kovski P, Kratzel A, Steiner S, Stalder H, Thiel V. Coronavirus biology and replication: implications for SARS-CoV-2. Nature Reviews Microbiology. 2020.
28. Ward P. COVID-19/SARS-CoV-2 pandemich. Faculty of pharmaceutical medicine blod. 2020;6th april
29. Du L, He Y, Zhou Y, Liu S, Zheng B-J, Jiang S. The spike protein of SARS-CoV — a target for vaccine and therapeutic development. Nature Reviews Microbiology. 2009;7(3):226-36.
30. Folkehelseinstituttet (FHI). Testkriterier for koronavirus (coronavirus) [internet]. 2020 [updated 27.11.2020; cited 2020 29th november]. Available from: https://www.fhi.no/nettpub/coronavirus/testing-og-oppfolging-av-smittede/testkriterier/.
31. Vandenberg O, Martiny D, Rochas O, van Belkum A, Kozlakidis Z. Considerations for diagnostic COVID-19 tests. Nature Reviews Microbiology. 2020.
32. Folkehelseinstituttet (FHI). Antigentester Oslo 2020 [Available from: https://www.fhi.no/nettpub/coronavirus/testing-og-oppfolging-av-smittede/hurtigtester-for-pavisning-av-koronavirus/.
33. T10.3.5.2 Covid-19/koronavirus legemiddelhåndbok N, editor. oslo Norsk Legemiddelhåndbok 2021 28.03.2021.
34. Vabret N, Britton GJ, Gruber C, Hegde S, Kim J, Kuksin M, et al. Immunology of COVID-19: Current State of the Science. Immunity. 2020;52(6):910-41.
35. Chau AS, Weber AG, Maria NI, Narain S, Liu A, Hajizadeh N, et al. The Longitudinal Immune Response to Coronavirus Disease 2019: Chasing the Cytokine Storm. Arthritis Rheumatol. 2020.
36. Schulte-Schrepping J, Reusch N, Paclik D, Baßler K, Schlickeiser S, Zhang B, et al. Severe COVID-19 Is Marked by a Dysregulated Myeloid Cell Compartment. Cell. 2020;182(6):1419-40.e23.
37. Vabret N, Britton GJ, Gruber C, Hegde S, Kim J, Kuksin M, et al. Immunology of COVID-19: Current State of the Science. Immunity. 2020;52(6):910-41.
38. Melenotte C, Silvin A, Goubet A-G, Lahmar I, Dubuisson A, Zumla A, et al. Immune responses during COVID-19 infection. OncoImmunology. 2020;9(1):1807836.
39. Rijkers G, Vervenne T, van der Pol P. More bricks in the wall against SARS-CoV-2 infection: involvement of γ9δ2 T cells. Cellular & Molecular Immunology. 2020;17(7):771-2.
40. Lei L, Qian H, Yang X, Zhang X, Zhang D, Dai T, et al. The phenotypic changes of γδ T cells in COVID-19 patients. Journal of Cellular and Molecular Medicine. 2020;24(19):11603-6.
41. Braun J, Loyal L, Frentsch M, Wendisch D, Georg P, Kurth F, et al. SARS-CoV-2-reactive T cells in healthy donors and patients with COVID-19. Nature. 2020;587(7833):270-4.
42. Poland GA, Ovsyannikova IG, Kennedy RB. SARS-CoV-2 immunity: review and applications to phase 3 vaccine candidates. The Lancet. 2020.
43. Spitzer MH, Nolan GP. Mass Cytometry: Single Cells, Many Features. Cell. 2016;165(4):780-91.
44. Bandura DR, Baranov VI, Ornatsky OI, Antonov A, Kinach R, Lou X, et al. Mass cytometry: technique for real time single cell multitarget immunoassay based on inductively coupled plasma time-of-flight mass spectrometry. Anal Chem. 2009;81(16):6813-22.

45. Bjornson ZB, Nolan GP, Fantl WJ. Single-cell mass cytometry for analysis of immune system functional states. Curr Opin Immunol. 2013;25(4):484-94.
46. Fluidigm. Helios, A CyTOF System. In: Corporation F, editor. Internet Verison 7 ed. Canada Fluidigm Corporation; 2018.
47. Bendall SC, Nolan GP, Roederer M, Chattopadhyay PK. A deep profiler's guide to cytometry. Trends Immunol. 2012;33(7):323-32.
48. Wilschefski SC, Baxter MR. Inductively Coupled Plasma Mass Spectrometry: Introduction to Analytical Aspects. Clin Biochem Rev. 2019;40(3):115-33.
49. Bringeland GH. A mass cytometry receptor occupancy study of natalizumab therapy in multiple sclerosis. 2020.
50. Hartmann FJ, Simonds EF, Bendall SC. A Universal Live Cell Barcoding-Platform for Multiplexed Human Single Cell Analysis. Scientific Reports. 2018;8(1):10770.
51. Fluidigm. Cell-OD 20-Plex Pd barcoding Kit: user guide. Fluidigm San Francisco, CA, USA: Fluidigm; 2019.
52. Zunder ER, Finck R, Behbehani GK, Amir E-AD, Krishnaswamy S, Gonzalez VD, et al. Palladium-based mass tag cell barcoding with a doublet-filtering scheme and single-cell deconvolution algorithm. Nat Protoc. 2015;10(2):316-33.
53. Bio-Rad-Antibodies. Why is antibody titration important? oslounkown [cited 2021 31st january]. Available from: https://www.bio-rad-antibodies.com/flow-antibody-titration.html?JSESSIONID_STERLING=C4418571C8409841A2F1391B76F8C32B.ecommerce1&evCntryLang=NO-en&cntry=NO&thirdPartyCookieEnabled=true.
54. Palit S, Heuser C, de Almeida GP, Theis FJ, Zielinski CE. Meeting the Challenges of High-Dimensional Single-Cell Data Analysis in Immunology. Front Immunol. 2019;10:1515-.
55. Kimball AK, Oko LM, Bullock BL, Nemenoff RA, van Dyk LF, Clambey ET. A Beginner's Guide to Analyzing and Visualizing Mass Cytometry Data. J Immunol. 2018;200(1):3-22.
56. Amir E-aD, Lee B, Badoual P, Gordon M, Guo XV, Merad M, et al. Development of a Comprehensive Antibody Staining Database Using a Standardized Analytics Pipeline. Front Immunol. 2019;10(1315).
57. Sigma A. Protocol Guide: MTT assay for cell viability and proliferation 2020 [cited 2021 02.03]. Available from: https://www.sigmaaldrich.com/technical-documents/protocols/biology/roche/cell-proliferation-kit-i-mtt.html.
58. Iglesias DE, Cremonini E, Fraga CG, Oteiza PI. Ellagic acid protects Caco-2 cell monolayers against inflammation-induced permeabilization. Free Radical Biology and Medicine. 2020;152:776-86.
59. PubChem Compound Summary for CID 5281855, Ellagic acid Internet National Center for Biotechnology Information (2021). 2021 [Available from: https://pubchem.ncbi.nlm.nih.gov/compound/Ellagic-acid.
60. Opretzka LCF, Espírito-Santo RFd, Nascimento OA, Abreu LS, Alves IM, Döring E, et al. Natural chromones as potential anti-inflammatory agents: Pharmacological properties and related mechanisms. International Immunopharmacology. 2019;72:31-9.
61. Kim DS, Woo ER, Chae SW, Ha KC, Lee GH, Hong ST, et al. Plantainoside D protects adriamycin-induced apoptosis in H9c2 cardiac muscle cells via the inhibition of ROS generation and NF-kappaB activation. Life Sci. 2007;80(4):314-23.
62. Koh HLAC, Tung Kian%A Tan, Chay Hoon. A Guide to Medicinal Plants.
63. Van Gassen S, Callebaut B, Van Helden MJ, Lambrecht BN, Demeester P, Dhaene T, et al. FlowSOM: Using self-organizing maps for visualization and interpretation of cytometry data. Cytometry Part A. 2015;87(7):636-45.
64. Rodriguez L, Pekkarinen PT, Lakshmikanth T, Tan Z, Consiglio CR, Pou C, et al. Systems-Level Immunomonitoring from Acute to Recovery Phase of Severe COVID-19. Cell Rep Med. 2020;1(5):100078.
65. Dan JM, Mateus J, Kato Y, Hastie KM, Yu ED, Faliti CE, et al. Immunological memory to SARS-CoV-2 assessed for up to 8 months after infection. Science. 2021;371(6529):eabf4063.

66. Wang F, Nie J, Wang H, Zhao Q, Xiong Y, Deng L, et al. Characteristics of Peripheral Lymphocyte Subset Alteration in COVID-19 Pneumonia. J Infect Dis. 2020;221(11):1762-9.
67. Silvin A, Chapuis N, Dunsmore G, Goubet AG, Dubuisson A, Derosa L, et al. Elevated Calprotectin and Abnormal Myeloid Cell Subsets Discriminate Severe from Mild COVID-19. Cell. 2020;182(6):1401-18.e18.
68. Ożańska A, Szymczak D, Rybka J. Pattern of human monocyte subpopulations in health and disease. Scandinavian Journal of Immunology. 2020;92(1):e12883.
69. Casanova JL, Su HC. A Global Effort to Define the Human Genetics of Protective Immunity to SARS-CoV-2 Infection. Cell. 2020;181(6):1194-9.
70. Parker CM, Groh V, Band H, Porcelli SA, Morita C, Fabbi M, et al. Evidence for extrathymic changes in the T cell receptor gamma/delta repertoire. J Exp Med. 1990;171(5):1597-612.
71. Shuwa HA, Shaw TN, Knight SB, Wemyss K, McClure FA, Pearmain L, et al. Alterations in T and B cell function persist in convalescent COVID-19 patients. Med. 2021.
72. Newell KL, Clemmer DC, Cox JB, Kayode YI, Zoccoli-Rodriguez V, Taylor HE, et al. Switched and unswitched memory B cells detected during SARS-CoV-2 convalescence correlate with limited symptom duration. medRxiv. 2020:2020.09.04.20187724.
73. Brodin P, Duffy D, Quintana-Murci L. A Call for Blood—In Human Immunology. Immunity. 2019;50(6):1335-6.
74. Silva MH, Lepzien R, Ols S, Dahlberg B, Grunewald J, Loré K, et al. Stabilization of blood for long-term storage can affect antibody-based recognition of cell surface markers. Journal of Immunological Methods. 2020;481-482:112792.
75. Yokoyama WM, Thompson ML, Ehrhardt RO. Cryopreservation and thawing of cells. Curr Protoc Immunol. 2012;Appendix 3:3g.
76. Fjaeraa C, Nånberg E. Effect of ellagic acid on proliferation, cell adhesion and apoptosis in SH-SY5Y human neuroblastoma cells. Biomedicine & Pharmacotherapy. 2009;63(4):254-61.
77. Byrne JD, Betancourt T, Brannon-Peppas L. Active targeting schemes for nanoparticle systems in cancer therapeutics. Adv Drug Deliv Rev. 2008;60(15):1615-26.
78. Kumar N, Afjei R, Massoud TF, Paulmurugan R. Comparison of cell-based assays to quantify treatment effects of anticancer drugs identifies a new application for Bodipy-L-cystine to measure apoptosis. Scientific Reports. 2018;8(1):16363.
79. Wang P, Henning SM, Heber D. Limitations of MTT and MTS-based assays for measurement of antiproliferative activity of green tea polyphenols. PloS one. 2010;5(4):e10202-e.
80. Li L-W, Na C, Tian S-Y, Chen J, Ma R, Gao Y, et al. Ellagic acid induces HeLa cell apoptosis via regulating signal transducer and activator of transcription 3 signaling. Exp Ther Med. 2018;16(1):29-36.
81. Kumar D, Basu S, Parija L, Rout D, Manna S, Dandapat J, et al. Curcumin and Ellagic acid synergistically induce ROS generation, DNA damage, p53 accumulation and apoptosis in HeLa cervical carcinoma cells. Biomed Pharmacother. 2016;81:31-7.
82. van Tonder A, Joubert AM, Cromarty AD. Limitations of the 3-(4,5-dimethylthiazol-2-yl)-2,5-diphenyl-2H-tetrazolium bromide (MTT) assay when compared to three commonly used cell enumeration assays. BMC Res Notes. 2015;8:47-.
83. Carreño EA, Alberto AVP, de Souza CAM, de Mello HL, Henriques-Pons A, Anastacio Alves L. Considerations and Technical Pitfalls in the Employment of the MTT Assay to Evaluate Photosensitizers for Photodynamic Therapy. Applied Sciences. 2021;11(6):2603.
84. Thermofisher. Useful information for various sizes of cell culture dishes and flasks internet: ThermoFisher Scinetific [cited 2021 24.04]. Available from: https://www.thermofisher.com/no/en/home/references/gibco-cell-culture-basics/cell-culture-protocols/cell-culture-useful-numbers.html.
85. Sarkar I. Towards startification of patients with Sjøgren's syndrome - Single cell analysis and immune profiling. Bergen University of Bergen; 2020.
86. Aarebrot AK. Single cell signaling and immune cell profiling in psoriasis Skipnes Kommunikasjon: Univeristy of Bergen 2021.

Supplementary

Table S1 Raw data, standard deviation, coefficient of variable for triplicates for Ellagic acid in HEK293t

Concentration (mM)	Replicates			Mean	Standard deviation	CV
	1	2	3			
0	0	0	0	0	-	-
10^{-6}	0,508	0,441	0,464	0,471	0,034	13,835
10^{-5}	0,709	0,505	0,558	0,591	0,106	5,580
10^{-4}	1,007	0,708	0,926	0,880	0,155	5,693
10^{-3}	1,105	1,048	1,018	1,057	0,044	23,918
10^{-2}	1,191	1,174	1,154	1,173	0,019	63,336
0,1	0,826	1,072	1,034	0,977	0,132	7,380
1	0,517	0,49	0,494	0,500	0,015	34,336
10	0,329	0,341	0,36	0,343	0,016	21,965

Table S2 Raw data, standard deviation, coefficient of variable for triplicates for Rumic acid in HEK293t

Concentration	Replicates			Mean	Standard deviation	CV
	1	2	3			
0	0	0	0	0	0,000	-
10^{-6}	-	-	-	-	-	-
10^{-5}	0,461	0,479	0,472	0,471	0,009	51,871
10^{-4}	0,608	0,658	0,683	0,650	0,038	17,012
10^{-3}	1,017	0,986	1,094	1,032	0,056	18,564
10^{-2}	1,17	1,137	1,035	1,114	0,070	15,829
0,1	1,207	1,26	1,07	1,179	0,098	12,025
1	1,143	1,139	0,968	1,083	0,100	10,844
10	1,196	1,123	1,078	1,132	0,060	19,014

Table S3 Raw data, standard deviation, coefficient of variable for triplicates for Dinatin 7-Glucuriode in HEK293t

Concentration	Replicates			Mean	Standard deviation	CV
	1	2	3			
0	0	0	0	0	0,000	-
10^{-7}	0,31	0,377	0,324	0,337	0,035	9,536
10^{-6}	0,387	0,381	0,422	0,397	0,022	17,913
10^{-5}	0,526	0,525	0,59	0,547	0,037	14,688
10^{-4}	0,898	0,958	0,939	0,932	0,031	30,382
10^{-3}	1,077	1,146	1,013	1,079	0,067	16,217
10^{-2}	1,016	1,2	0,921	1,046	0,142	7,372
0,1	0,921	0,981	0,799	0,900	0,093	9,708
1	0,803	0,773	0,71	0,762	0,047	16,054

Table S4 Raw data, standard deviation, coefficient of variable for triplicates for plantainoside D in HEK293t

Concentration	Replicates			Mean	Standard deviation	CV
	1	2	3			
0	0	0	0	0,000	0,000	-
10^{-6}	0,949	0,545	0,614	0,703	0,216	3,252
10^{-5}	1,013	0,785	0,784	0,861	0,132	6,524
10^{-4}	1,031	0,999	0,97	1,000	0,031	32,774
10^{-3}	0,924	0,926	0,838	0,896	0,050	17,835
10^{-2}	0,936	0,934	0,751	0,874	0,106	8,224
0,1	0,67	0,766	0,358	0,598	0,213	2,803
1	0,287	0,329	0,325	0,314	0,023	13,532

Table S5 Raw data, standard deviation, coefficient of variable for triplicates for Ellagic acid in HEK293

Concentration	Replicates			Mean	Standard deviation	CV
	1	2	3			
0	0	0	0	0	0,000	-
10^{-6}	1,136	0,872	1,004	1,004	0,132	7,606
10^{-5}	1,182	0,971	1,039	1,064	0,108	9,879
10^{-4}	1,167	0,938	1,019	1,041	0,116	8,968
10^{-3}	1,053	0,826	0,494	0,791	0,281	2,814
10^{-2}	1,041	0,774	0,632	0,816	0,208	3,928
0,1	1,142	0,819	0,423	0,795	0,360	2,207
1	0,769	0,57	0,432	0,590	0,169	3,484
10	0,302	0,308	0,267	0,292	0,022	13,202

Table S6 Raw data, standard deviation, coefficient of variable for triplicates for rumic acid in HEK293

Concentration	Replicates			Mean	Standard deviation	CV
	1	2	3			
0	0	0	0	0	0,000	-
10^{-6}	-	-	-	-	-	-
10^{-5}	1,148	1,279	1,238	1,222	0,067	18,231
10^{-4}	1,08	1,241	1,348	1,223	0,135	9,066
10^{-3}	0,942	1,176	1,259	1,126	0,164	6,848
10^{-2}	0,942	1,067	1,136	1,048	0,098	10,661
0,1	1,001	1,078	1,223	1,101	0,113	9,764
1	1,061	1,15	1,252	1,154	0,096	12,078
10	1,344	1,35	1,462	1,385	0,066	20,844

Table S7 Raw data, standard deviation, coefficient of variable for triplicates for Dinatin 7-glucuronide in HEK293

Concentration	Replicates			Mean	Standard deviation	CV
	1	2	3			
0	0	0	0	0	0,000	-
10^{-7}	1,147	1,323	1,152	1,207	0,100	12,049
10^{-6}	1,352	1,209	1,223	1,261	0,079	16,000
10^{-5}	1,382	1,24	1,445	1,356	0,105	12,910
10^{-4}	1,261	1,382	1,328	1,324	0,061	21,837
10^{-3}	1,062	1,314	1,123	1,166	0,131	8,871
10^{-2}	1,283	1,15	1,188	1,207	0,069	17,619
0,1	1,286	1,107	1,172	1,188	0,091	13,115
1	1,193	1,129	1,149	1,157	0,033	35,338

Table S8 Raw data, standard deviation, coefficient of variable for triplicates for plantainoside D in HEK293

Concentration	Replicates			Mean	Standard deviation	CV
	1	2	3			
0	0	0	0	0,000	0,000	-
10^{-6}	-	-	-	-	-	-
10^{-5}	0,908	0,751	0,752	0,804	0,090	8,894
10^{-4}	0,997	0,857	0,826	0,893	0,091	9,805
10^{-3}	1,061	0,886	0,899	0,949	0,098	9,730
10^{-2}	1,242	1,209	1,094	1,182	0,078	15,209
0,1	1,384	1,34	1,231	1,318	0,079	16,737
1	1,339	1,195	1,184	1,239	0,086	14,329
10	1,343	1,243	0,977	1,188	0,189	6,278

Table S9 Raw data, standard deviation, coefficient of variable for triplicates for ellagic acid in CACO-2

Concentration	Replicates			Mean	Standard deviation	CV
	1	2	3			
0	0	0	0	0	0,000	-
10^{-6}	0,827	0,793	0,842	0,821	0,025	32,687
10^{-5}	0,818	0,712	0,599	0,710	0,110	6,480
10^{-4}	0,819	0,699	0,817	0,778	0,069	11,327
10^{-3}	0,677	0,7	0,864	0,747	0,102	7,325
10^{-2}	0,598	0,526	0,754	0,626	0,117	5,371
0,1	0,38	0,412	0,648	0,480	0,146	3,279
1	0,475	0,488	0,651	0,538	0,098	5,486
10	0,361	0,331	0,374	0,355	0,022	16,113

Table S10 Raw data, standard deviation, coefficient of variable for triplicates for Rumic acid in CACO-2

Concentration	Replicates			Mean	Standard deviation	CV
	1	2	3			
0	0	0	0	0	0,000	-
10^{-6}	-	-	-	-	-	-
10^{-5}	0,672	0,599	0,595	0,622	0,043	14,349
10^{-4}	0,688	0,541	0,618	0,616	0,074	8,373
10^{-3}	0,709	0,633	0,681	0,674	0,038	17,544
10^{-2}	0,709	0,65	0,649	0,669	0,034	19,482
0,1	0,7	0,612	0,638	0,650	0,045	14,377
1	0,747	0,714	0,721	0,727	0,017	41,830
10	0,831	0,861	0,836	0,843	0,016	52,428

Table S11 Raw data, standard deviation, coefficient of variable for triplicates for Dinatin 7-glucuroide in CACO-2

Concentration	**Replicates**			**Mean**	**Standard deviation**	**CV**
	1	2	3			
0	0	0	0	0	0,000	-
10^{-7}	0,834	0,74	0,779	0,784	0,047	16,608
10^{-6}	0,83	0,804	0,684	0,773	0,078	9,921
10^{-5}	0,726	0,644	0,7	0,690	0,042	16,466
10^{-4}	0,75	0,677	0,691	0,706	0,039	18,223
10^{-3}	0,782	0,756	0,72	0,753	0,031	24,175
10^{-2}	0,763	0,762	0,778	0,768	0,009	85,649
0,1	0,757	0,73	0,753	0,747	0,015	51,241
1	0,729	0,711	0,732	0,724	0,011	63,745

Table S12 Raw data, standard deviation, coefficient of variable for triplicates for plantainoside D in CACO-2

Concentration	**Replicates**			**Mean**	**Standard deviation**	**CV**
	1	2	3			
0	0	0	0	0	0,000	-
10^{-6}	-	-	-	-	-	-
10^{-5}	0,763	0,708	0,515	0,662	0,130	5,083
10^{-4}	0,784	0,602	0,493	0,626	0,147	4,260
10^{-3}	0,709	0,554	0,699	0,654	0,087	7,539
10^{-2}	0,695	0,583	0,661	0,646	0,057	11,256
0,1	0,678	0,699	0,609	0,662	0,047	14,060
1	0,843	0,737	0,595	0,725	0,124	5,826
10	0,904	0,891	0,721	0,839	0,102	8,213

Table S13 Antibody panel information

Antibody	**Clone**	**Metal**
CD45	HI30	89Y
CD57	HCD57	142 Nd
CD45RA	HI100	143 Nd
CD4	RPA-T4	145 Nd
IgD	IA6-2	146 Nd
CD20	2H7	147Sm
IgA	Polyclonal	148Nd
CD25	2A3	149Sm
CD123	6H6	151Eu
CD66b	80H3	152Sm
TCRg/d	11F2	152Sm
CD62L	DREG56	153Eu
CD366	D5D5R	154Sm
CD27	LI28	155Gd
CD11c	BU15	159Tb
CD14	RMO52	160Gd
CD152	14D3	161Dy
CD8	RPA-T8	162Dy
CD56	NCAM16.2	163Dy
CD161	HP-3G10	164Dy
CD45RO	UCHL1	165Ho
CD11b	ICRF44	167Er
CD19	BTG	169Tm
CD3	UCHT1	170Er
CD38	HIT2	172Yb
CD141	1A4	173Yb
HLA-DR	L243	174Yb
CD279	PD-1	175Lu
CD127	A019D5	176Yb
CD16	3G8	209Bi